

UNIFICATION OF THE FUNDAMENTAL PLANE AND SUPER-MASSIVE BLACK HOLES MASSES

REMCO C. E. VAN DEN BOSCH (BOSCH@MPIA.DE)

Accepted by ApJ. In original form on February 29th 2016. Third revision submitted on June 20rd. Current revision 2016/06/23.

Abstract

According to the Virial Theorem, all gravitational systems in equilibrium sit on a plane in the 3D parameter space defined by their mass, size and second moment of the velocity tensor. While these quantities cannot be directly observed, there are suitable proxies: the luminosity L_k , half-light radius R_e and dispersion σ_e . These proxies indeed lie on a very tight Fundamental Plane (FP). How do the black holes in the centers of galaxies relate to the FP? Their masses are known to exhibit no strong correlation with total galaxy mass, but they do correlate weakly with bulge mass (when present), and extremely well with the velocity dispersion through the $M_\bullet \propto \sigma_e^{5.4}$ relation. These facts together imply that a tight plane must also exist defined by black hole mass, total galaxy mass and size. Here I show that this is indeed the case using a heterogeneous set of 230 black holes. The sample includes BHs from zero to 10 billion solar masses and host galaxies ranging from low surface brightness dwarfs, through bulge-less disks, to brightest cluster galaxies. The resulting BH–size–luminosity relation $M_\bullet \propto (L_k/R_e)^{3.8}$ has the same amount of scatter as the M_\bullet – σ relation and is aligned with the galaxy FP, such that it is just a re-projection of σ_e . The inferred BH–size–mass relation is $M_\bullet \propto (M_*/R_e)^{2.9}$. These relationships are universal and extend to galaxies without bulges. This implies that the black hole is primarily correlated with its global velocity dispersion and not with the properties of the bulge. I show that the classical bulge–mass relation is a projection of the M_\bullet – σ relation. When the velocity dispersion cannot be measured (at high- z or low dispersions), the BH–size–mass relation should be used as a proxy for black hole mass in favor of just galaxy or bulge mass.

Table and code available at <https://github.com/remcovandenbosch/Black-Hole-Mass-compilation>.

1. DYNAMICAL SCALING RELATIONS

The Virial Theorem states that all gravitational systems in equilibrium sit on a plane $GM_{1/2} = R_{1/2}\sigma_{1/2}^2$ in the 3D parameter space defined by half of the mass, the size and the second moment of the velocity tensor of those systems. While we cannot directly observe these quantities, we do have suitable proxies: the luminosity, half-light radius R_e and stellar velocity dispersion σ_e . Together these three variables define the Fundamental Plane (Djorgovski & Davis 1987; Dressler et al. 1987) of early-type galaxies as is expected from the Virial Theorem. There are several empirical relationships that are understood to be projections of the Fundamental Plane: ellipticals follow the Faber-Jackson (1976) and Kormendy (1977) relations, and all early-type galaxies lie on a narrow red sequence (Chen et al. 2010). Spiral galaxies follow different dynamical scaling relations, including the Tully-Fisher (1977) relation linking galaxy luminosity to the circular velocity V_c measured at large radii ($> R_e$), which is typically used as a proxy for dark matter halo mass. All of these dynamical scaling relations are remarkably tight and can be used to measure galaxy masses and distances (see Courteau et al. 2014 for a review).

Host galaxy properties also correlate with the mass of the super-massive black holes (BHs) in their centers (see Kormendy & Ho (2013) for a review). Out of all BH scaling relations (none of which is as tight as the Fundamental Plane), the so-called M_\bullet – σ relation has been firmly established as the strongest, most universal relation (Gebhardt et al. 2003; Beifiori et al. 2012). This empirical relation between BH mass (M_\bullet) and velocity dispersion, shown in figure 1, has the least scatter of all other BH scaling relations. It applies to galaxies of all types, including the most massive galaxies – like M87 – and dwarf galaxies, such as local group members M33 and NGC205. There are only few outliers to the M_\bullet – σ relation. In the compilation of galaxies studied in this paper, the most no-

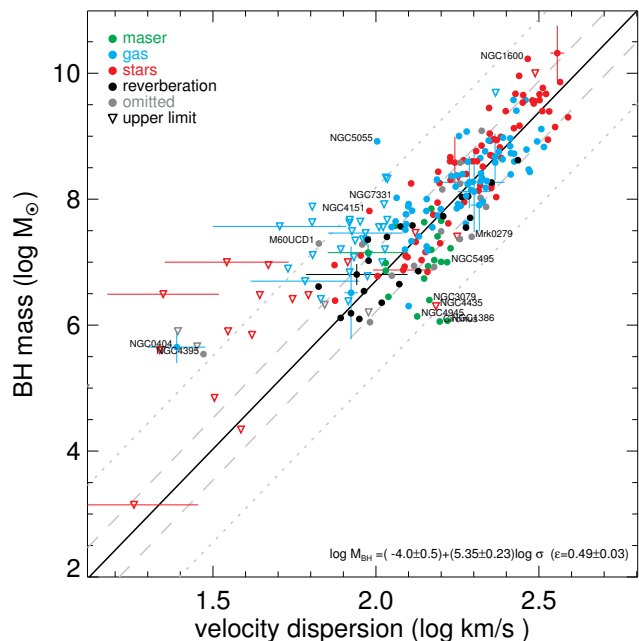


Figure 1. The tight correlation between black hole mass and stellar velocity dispersion. This solid line shows the M_\bullet – σ relation derived in §4. It is based on 230 galaxies spanning from dwarfs to brightest ellipticals. The scatter in this relation is ($\epsilon = 0.49 \pm 0.03$). Upper limits are shown as open triangles. Different colors denote different types of M_\bullet measurement (§2). Error bars for the objects with the largest uncertainties. The grey dashed and dotted lines denote 1 and 3 times the intrinsic scatter.

table outliers are the $10^6 M_\odot$ BHs from water masers (Greene et al. 2010, 2016; Kuo et al. 2011, §5.1). The galaxy with the smallest BH is M33 (=NGC598). The putative BH in this object has an upper limit on its mass of $1500 M_\odot$ (Gebhardt

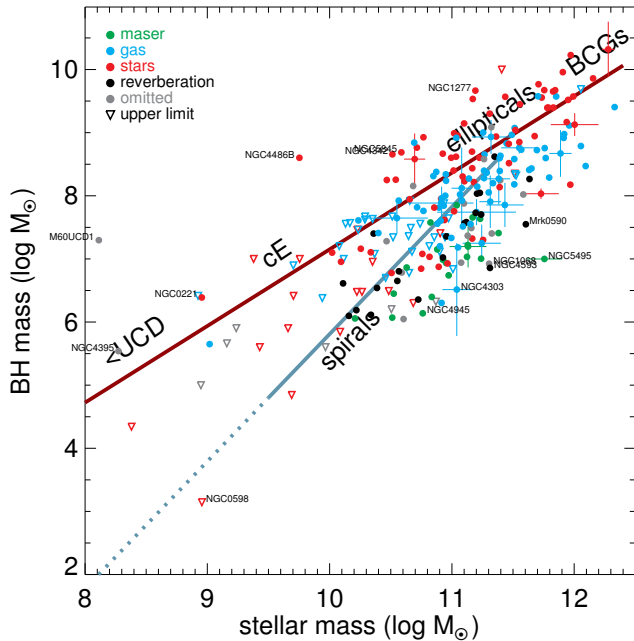


Figure 2. Total stellar mass and BH mass do not correlate well, as is shown here. The scatter of a simple regression (tab. 1) is ($\epsilon = 0.84 \pm 0.05$), which is significantly larger than on the M_\bullet - σ relation. However the distribution of points make the interpretation as a single powerlaw difficult (Reines & Volonteri 2015). Near $10^{11} M_\odot$ the BH mass varies by 3 orders of magnitude. Many different interpretations exist for subsets of galaxies and/or their bulges. The (compact) ellipticals – and classical bulges – appear to follow the red line. And the low mass (disk) galaxies appear to follow the blue line. The two populations converge near $10^{11} M_\odot$. See section 6 for the different projections of these scaling relations. The symbols are the same as in figure 1.

et al. 2001; Merritt et al. 2001). Considering the amount of scatter about the M_\bullet - σ relation, even these outliers are not especially far off the relation.

There is only one empirical relation tighter than the M_\bullet - σ relation, but this applies only to a small subset of galaxies: in the most massive bulge-dominated ellipticals, BH mass is correlated with bulge mass (e.g. Häring & Rix 2004; Gültekin et al. 2009a; Kormendy et al. 2011; Läscher et al. 2014b). Since not all galaxies have a bulge, the M_\bullet - σ relation is more generally applicable. The relevance of the empirical ‘black hole-bulge’ mass relation is also questionable in the case of the *pseudo*-bulges in disk galaxies, which do not correlate with black hole mass in the same way (Hu 2009; Jiang et al. 2011; Graham & Scott 2013), if at all (Sani et al. 2011; Kormendy et al. 2011; Läscher et al. 2016; Saglia et al. 2016). It should be noted, though, that comparative bulge studies are complicated by the difficulties of bulge and disk photometric decompositions, which are notoriously degenerate (e.g. Läscher et al. 2014a) and depend on non-unique definitions of what a bulge is (Kormendy & Kennicutt 2004).

A much more compelling correlation would avoid the bulge altogether and link BH mass directly with total galaxy mass (Figure 2). More massive galaxies do indeed have bigger black holes. However, the manner in which observed objects populate M_\bullet - M_\bullet space makes it difficult to claim that a single power law can accurately describe the correlation. At host galaxy masses near $10^{11} M_\odot$ the BH mass varies by 3 orders of magnitude. The AGNs appear to be offset from the ellipticals by an order of magnitude (Reines & Volonteri 2015). The over-massive black holes in bulge-dominated galaxies are also outliers (e.g. M60UCD-1, NGC1271, NGC1277 and

NGC4486B; Seth et al. 2014; Walsh et al. 2015, 2016; Saglia et al. 2016). The only galaxies that appear tight are the ellipticals (Kormendy & Ho 2013; Läscher et al. 2014b). Thus, all available evidence suggests that there is no clear universal relationship between BH and galaxy mass. The M_\bullet - σ arguably provides the much better predictor of BH mass.

Several other empirical relations have been considered in the literature, but most of these are just manifestations of the simple rule that more massive galaxies have bigger black holes (e.g. NSC mass, core radius, globular clusters, Sérsic n , pitch angle: Ferrarese et al. 2006; Kormendy & Bender 2009; Harris & Harris 2011; Savorgnan et al. 2013; Berrier et al. 2013). None of these relationships are tighter – or have less scatter – than M_\bullet - σ over the whole mass range (see the review by Graham (2016) and references therein). Notably, the circular velocity does not correlate well with BH mass (Ho 2007; Kormendy & Bender 2011; Sun et al. 2013), which is curious as it implies that the dark matter halo mass does not correlate with BH mass.

So far there have been very few satisfying multi-variate studies of BH scaling relations. Studies that consider additional parameters have mostly focused on the Black Hole Fundamental Plane¹ by adding bulge parameters, like bulge size or mass (e.g. Feoli & Mancini 2009; Marconi & Hunt 2003; Hu 2009; Aller & Richstone 2007; Hopkins et al. 2007b; Sani et al. 2011; Graham 2008; Saglia et al. 2016) to the M_\bullet - σ relation. The most exhaustive multi-variate search was done by Beifiori et al. (2012), who confirmed that the M_\bullet - σ was the best single-parameter relation. They could only marginally improve it by adding R_e as the secondary parameter.

If M_\bullet - σ is the best single-variate relation, what does σ truly represent? The total stellar mass does not correlate tightly with BH mass. Not all host galaxies have bulges. Alternative interpretations for M_\bullet - σ must therefore be investigated. Here, I undertake a new multi-variate study of BH scaling relations and examine the link between M_\bullet - σ and the global photometric properties of BH host galaxies. Beginning with a section on the data & methods, I describe the sample selection and the measurements of total luminosities and half-light radii. The regression fitting technique is described later in section 2.3. Then, in section 3 I first show that, for the adopted sample, the BH host galaxies themselves lie on a tight Fundamental Plane. I then confirm that the M_\bullet - σ is indeed the best single-parameter regression in section 4. Section 5.1 explores whether the M_\bullet - σ is internally consistent with the host galaxy Fundamental Plane identified in section 3 and then establishes the BH–size–luminosity relation, using stellar masses estimated using the mass-to-light conversion described in section 5.2.1. Finally, I discuss the implications for BH scaling relations for different types of galaxies in section 6 and conclude in section 7. Throughout, I adopt a flat concordance cosmology with $H_0 = 70 \text{ km s}^{-1}$ and $\Omega_m = 0.3$.

2. DATA AND METHODS

This section provides details on the construction of the sample of BH masses and host galaxy properties used in this work, as well as the methods employed for regression-fitting. A brief summary is included below and in subsection 2.2, which should be sufficient for most readers (who may want to skip the more technical details that follow).

To achieve proper leverage on the scaling relations, a large dynamic range in BH masses and host galaxy properties is

¹ Perhaps the Black Hole Bulge Plane would be a better name?

essential. In this work this is achieved with a sample of 230 galaxies compiled from the literature. For each object there is a black hole mass measurement in which the BH is either dynamically or temporally resolved. The galaxies and their properties are listed in table 2 and 3. Additional parameters and code for generating the figures and fits are available at <https://github.com/remcovandenbosch/Black-Hole-Mass-compilation>. The BH masses in this compilation come from four different methods: stellar dynamics, gas dynamics, megamasers and reverberation mapping. Each of these methods uses a different dynamical tracer and probes a different region in the potential well of the galaxy (e.g. Peterson 2014; Kormendy & Ho 2013; Walsh et al. 2013; van den Bosch et al. 2016). To highlight any potential biases that result, the symbol colour in all figures indicates the method used.

The sample under consideration is a factor two larger than most previous compilations (except Beifiori et al. 2012). This makes it possible to investigate regions of parameter space ($M_{\bullet} < 10^6 M_{\odot}$ and diffuse galaxies) that otherwise would not be probed. The local group dwarf galaxies M33 and NGC205 especially help characterize the low mass end.

The reader is cautioned that the mass measurements and their underlying assumptions – especially pertaining to stellar dynamics – are different for each measurement and, as a result, the sample is very heterogeneous. When different methods are applied to the same galaxy the results do differ (for a discussion see Walsh et al. 2013; van den Bosch et al. 2016). In addition, the biases of detecting a BH mass as well as null-results are a potential issue (Ferrarese & Ford 2005; Batcheldor 2010; Gültekin et al. 2011). Black hole masses can only be measured dynamically in galaxies that are extremely nearby and it is much easier to find bigger black holes than smaller ones (van den Bosch et al. 2015). Next generation facilities will significantly expand the parameter space (Davis 2014; Do et al. 2014). For now, although sample heterogeneity will certainly impact the scatter on the resulting black hole scaling relationships, this is not of particular relevance for this work, which focuses on the exploring the connection between the different relationships. As long as all fits are performed on the same sample they can be compared in a relative sense.

2.1. The Black Holes

The basis of the sample consists of the 97 galaxies from the [online compilation \(link\)](#) by McConnell & Ma (2013). These are all objects hosting black holes whose masses are measured with some kind of dynamical models in which the kinematic tracer have been spatially resolved. Added to that are four objects from the Gültekin et al. (2009b) compilation, another four from the Kormendy & Ho (2013) compilation and fifteen from Saglia et al. (2016). An additional 39 objects have (updated) black hole mass (upper limits) from Gebhardt et al. (2001), Merritt et al. (2001), Valluri et al. (2005), Barth et al. (2009), Kormendy et al. (2010), Seth et al. (2010), Neumayer & Walcher (2012), Lyubenova et al. (2013), De Lorenzi et al. (2013), Scharwächter et al. (2013), Onken et al. (2014), Nguyen et al. (2014), Gültekin et al. (2014), Yıldırım et al. (2015), Onishi et al. (2015), Walsh et al. (2015), Seth et al. (2014), Walsh et al. (2016), Barth et al. (2016), Thomas et al. (2016), Greene et al. (2016) and Onishi et al. (2016). Another 80 objects with *HST*/*STIS* spectroscopy are added from Beifiori et al. (2009, 2012). The galaxies from Beifiori et al. (2009, 2012) with low dispersions were shown to appear systematically offset from the M_{\bullet} – σ and hence I treat those

objects with dispersions below 105 km s^{-1} as upper limits in this compilation.² The remainder is included as BH mass measurements.

Temporally resolved black holes. Also included in the sample are the 50 BH masses from Bentz & Katz (2015), for which the size of the broad emission-line region around the black hole is resolved using time lags by repeated observations. Only 24 of these objects are included in the analysis. The remainder of the host galaxies are not sufficiently bright or large enough for a robust growth curve with the 2MASS data (§ 2.2.1). The BH masses are scaled using the virial factor $\langle f \rangle$ of 4.31 ± 1.05 from Grier et al. (2013).³ The reverberation BH masses expand the sample towards lower black hole masses and shows that the AGN galaxies also follow the BH–size–luminosity relation.

Velocity dispersions. For compatibility with the Virial Theorem, the ideal measurement constraining the dynamical state of galaxies would be the second moment of the 3D velocity tensor inside the half light radius. However this is not directly observable in external galaxies. The closest is the measurement of the stellar velocity dispersion of all the combined spectra inside an aperture the size of the effective radius, as this is the 1D projection of the second moment. Inside the half-light radius the baryons dominate (See section 3 and 5.2.1).

The measurement of σ_e is most easily performed with an integral-field spectrograph (IFU, e.g. SAURON, Emsellem et al. 2004), by collapsing the entire spectrum inside $1 R_e$. However, IFU observations are not available for most of the sample. Different studies have used different definitions of σ to correlate with black hole mass. The widely used definition of σ_e from Gültekin et al. (2009b) adopts the luminosity-weighted average of $\langle V^2 + \sigma^2 \rangle$ per spatial kinematics bin inside one effective radius. This includes both the rotational V and the dispersion σ component of the velocity tensor (c.f. Bennert et al. 2011; Woo et al. 2013). This is often computed from long-slit observations (e.g. Bellovary et al. 2014). The M_{\bullet} – σ relation study by McConnell & Ma (2013) uses a similar definition, but excludes the central region inside the BHs gravitational sphere-of-influence, where the black hole influences the dispersion. Given that the BH is part of the self-gravitating system that the FP probes, this region should arguably be included in the computation of σ_e .

In the present compilation, for each galaxy the dispersion in the literature that most closely approximates σ_e is used (where available). The literature dispersion are superseded by the σ_e measurements from Cappellari et al. (2013b), Saglia et al. (2016), McConnell & Ma (2013) (in decreasing order of priority). When a dispersion is not otherwise available it is taken from Grier et al. (2013), van den Bosch et al. (2015). Notably, good σ_e 's are not available for the lowest-mass spirals. These particular galaxies are so nearby that their quoted literature dispersions are measured in the central arcseconds

² I speculate that the σ_e in the lowest mass galaxies of Beifiori et al. (2012) are underestimated, as they do not include the rotational part of the second moment (Falcón-Barroso et al. 2016). While their M_{\bullet} measurements are consistent with the BH–size–luminosity relation, their low dispersions make it appear that the BH masses lie above the M_{\bullet} – σ . The Fundamental Plane would indeed predict higher dispersions. See also §2.1 and §3.

³ Note that the $\langle f \rangle$ -factor is derived under the assumption that the AGN galaxies follow the M_{\bullet} – σ relation. As an independent consistency check of $\langle f \rangle$, I excluded all the reverberation mapped galaxies from the BH–size–luminosity relation fit (from §5.1) and then used the resulting regression to predict the black hole masses of the 26 reverberation mapped galaxies with growth curves. The weighted mean of the difference between that and the measured BH masses gives $\langle \log f \rangle = 0.62 \pm 0.04$. This is consistent with the adopted literature value.

only. Since the half-light radius for these systems is more than an order of magnitude larger, these dispersions do not include the contribution of the disk rotation into the second moment. To convert the σ of the lowest-mass spirals from Barth et al. (2009), Kormendy et al. (2010), and Neumayer & Walcher (2012) to σ_e , I adopt the aperture correction $\sigma_e/\sigma = (R/R_e)^{0.08}$ for spirals from CALIFA IFU observations following Falcón-Barroso et al. (2016). For these spirals, the correction is about 20% and is still relatively small with respect to the large dynamic range of the BH sample presented here. This correction is not applied to any other galaxies (see also footnote 2).

The literature dispersions are all measured with different instruments and methods and are often selected for study based on consistency with the relation (c.f. Jardel et al. 2011). Surprisingly, though, the inhomogeneity of these dispersions does not seem to impact the results; if the dispersions are in error, they would not yield the very tight fundamental plane shown in section 3. Note that small changes in the aperture size do not affect the dispersion significantly: $\sigma_e/\sigma = (R/R_e)^\alpha$, where $-0.06 < \alpha < 0.08$ (Falcón-Barroso et al. 2016).

Distances. Where possible in the sample I adopt the galaxy distances and their errors from the compilation by Saglia et al. (2016). The average distance uncertainty throughout that whole sample is 9%. For all other galaxies distances are taken from their literature sources. For these, an uncertainty of 10% is adopted unless an uncertainty is specifically quoted. The distances to local galaxies are relatively uncertain, due to the relatively large contribution of their peculiar velocities to the estimation of their redshifts, yielding high distance uncertainties. Unfortunately, redshift-independent distances are not available for most of these objects.

2.2. Photometry

In order to properly consider black hole masses in the context of the Virial Theorem – c.q. Fundamental Plane – global photometric properties are needed. The total near-infrared luminosity is a suitable proxy for the total stellar mass while the major axis length of the isophote containing half the light is a good proxy for half-light radius, as it is not strongly affected by projection effects. Almost all galaxies with a M_\bullet are close and bright enough such that the K_s -band imaging from the Two Micron All Sky Survey (2MASS, Skrutskie et al. 2006) is sufficient.⁴ The K_s -band is not very sensitive to dust or to changes in stellar mass-to-light ratio (Bell & de Jong 2001). In the infrared bands galaxy sizes are also smaller, i.e. than in optical bands, as a result of inside-out growth; at shorter wavelengths, the contribution from young optically bright stars leads to larger measured sizes.

Using the growth-curve method detailed in the next section, I measured the photometry of the 260 galaxies from the full sample that are both resolved ($R_e > 1''$) and adequately detected ($M_k < 11$) in 2MASS. This is the same selection cut as the parent sample used in the HETMGS (van den Bosch et al. 2015). They are listed in table 2. Only 30 objects in the present compilation do not fit these criteria. Many of these are reverberation-mapped AGN, which are either too dim or are effectively point sources in the 2MASS photometry. The objects without photometry are listed in table 3. In the other cases where the growth-curve analysis could not be performed, the catalog is augmented with photometric data from the 2MASS XSC (Jarrett et al. 2000) or Large Galaxy Atlas (Jarrett et al. 2003) or from the BH mass literature, when available. These

cases are recognizable in the data tables by the lack of uncertainties on their photometric values.

The growth-curve analysis provides non-parametric determinations of the galaxy luminosities, sizes, and concentration indices (and their covariances). This is achieved by fitting each galaxy multiple times with 3 Sérsic functions in which the outermost Sérsic n is varied. The Sérsic function is selected for its convenience and ability to fit galaxy photometry extremely well.

2.2.1. Sérsic growth curves

Three Sérsics for the Elven-kings under the sky,
Seven for the Dwarf-lords in their halls of stone,
Nine for Mortal Men doomed to die,
One for the Dark Lord on his dark throne,
In the Land of Galaxies where the Shadows lie,
One Sérsic for strong residuals, One Sérsic to fiat them,
Three Sérsics to bring them all and in the darkness bind them
In the Land of Sérsic-fits where the Shadows lie.

The Lord of the Sérsics, epigraph

In this section I describe the technical details of the photometric measurements. The 2MASS atlas images have dimensions of 512×1024 pixels of $1''$ each with a typical PSF size of $3''$ Full-Width-Half-Maximum (FWHM). To prepare for the Sérsic fitting, all the images are pre-processed with SEXTRACTOR (Bertin & Arnouts 1996), to find and mask all the stars and extended objects. Then a global PSF is constructed using PSFEX (Bertin 2011) that extends 30 times beyond the FWHM, with a plate scale of $0.5''$. The galaxies in the sample are much larger than the PSF, so fluctuations in the PSF core size are less relevant than the spiders and the coma of the PSF, especially when fitting the AGN cores and bright foreground stars. The central core of the PSF is governed by the subsampling of the $2''$ detector pixels onto the $1''$ output grid.

Next, an initial galaxy model is made with *galfit* (Peng et al. 2002) using the parameters from the 2MASS extended source catalog (XSC, Jarrett et al. 2000) as seed values. Each fit has been manually inspected to ensure a reasonable convergence. The model contains three Sérsics profiles for the galaxy, plus a central (non-thermal) point source (when an AGN is present) and a sky plane with variable tilt. Nearby bright stars and extended objects are unmasked and included while fitting the galaxy of interest as a point source and a single Sérsic, respectively. The fit is performed on a region ten times larger than the extent of the target galaxy. An example fit is shown in figure 3.

Several additional constraints aid numerical convergence: the luminosities of each Sérsic are required to be within 4 magnitudes of each other; all three Sérsic functions are constrained to have the same centroid position and position angle; the Sérsic indexes are required to be in the range $0.5 < n < 4$. The choice of these Sérsic profiles is driven by the desire to have enough freedom in the inner part and at the same time have an outer Sérsic for the growth curve. This appears to be the minimum required to fit the photometry without large residuals (Huang et al. 2013).

Starting with the initial galaxy model, *galfit* is run 100 times for the subsequent growth curve analysis. In each fit, the starting conditions – including the sky pedestal – are varied by 10% and the outer slope is varied by fixing the index n of the outer Sérsic from 0.5 to 4, in the 100 incremental steps.

⁴ Throughout the remainder of the paper K_s is shortened to K .

Additionally, the half-light radius of the outer Sérsic is forced to be at least 20% larger than the other Sérsics. This ensures that the outer-slope of the model is fixed to the intended value. This scheme essentially represents a ‘brute force approach’ to fitting growth curves with different slopes at large radii. As an example, the 100 surface brightness profiles of NGC3245 resulting from such a Monte-Carlo run is shown in figure 4.

The combined iterations provide a measure of the uncertainties and covariance of the parameters of the surface brightness profile. The total flux in the 3 Sérsics profiles represents the total galaxy luminosity. The half-light radius $R_e (=R_{50})$ is the major axis length of the isophote that contains 50% of the light in the deconvolved image. (Similarly, the radii R_{20} and R_{80} each contain 20% and 80% of the light, respectively.) To include uncertainty on the radius measurements, $0.5''$ scatter in the PSF FWHM is added⁵. Then the correlation matrix of the total luminosity, half-light radius and concentration $C_{28} = 5 \log R_{20}/R_{80}$ is computed.

The uncertainties on the photometric properties are strongly correlated and are not negligible. The median uncertainty on the total luminosity and half-light radius are 0.09 mag and 0.06 dex. The magnitudes are converted to solar luminosity L_K by adopting an absolute solar luminosity for the Sun of 3.28 magnitudes and a correction for the foreground extinction from Schlegel et al. (1998). All the measurements used in the fits presented in this paper are in table 2. Other numbers and covariances are [available online](#).

The Two Micron All Sky Survey is relatively shallow and

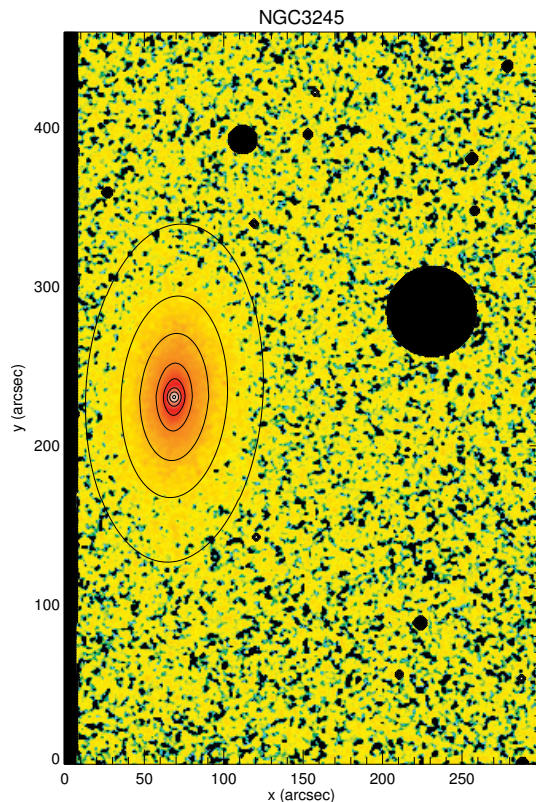


Figure 3. The 2MASS atlas image of NGC3245. Overplotted are the contours of equal surface brightness for the best-fit model in steps of 1 magnitude. Distant bright stars and galaxies are masked. Nearby stars and galaxies are added to fit. The images of the other galaxies are available in a figure set.

⁵ In practice this factor is negligible apart from the galaxies with the smallest apparent sizes, like NGC4486B.

thus the photometry does not resolve low surface brightness features. The sizes ($R_{K_R_EFF}$) and apparent magnitudes ($m_{K_M_EXT}$) tabulated in the XSC, in particular, are known to be underestimated (e.g. Lauer et al. 2007b; Cappellari et al. 2011). Figure 5 shows a comparison of total magnitudes measured here with values in the literature. Reassuringly, the photometry presented in this work is comparable to the very deep K-band photometry observed with CFHT/WIRCAM of 35 galaxies from Läsker et al. (2014a). As expected, there appears to be a significant offset between the growth-curves and the XSC. Using the technique from section 2.3, I find that the XSC magnitudes are significantly fainter than the 2D growth curves (i.e. the magnitude measured here $m_K = -0.33 + 1.01 m_{K_M_EXT}$), with inferred errors of $\delta m_{K_M_EXT} = 0.18$. The XSC apparent sizes are also significantly smaller, as expected. The best-fit transformation from those sizes to the values measured here with the growth-curve analysis is $\log R_e = 1.16 \log R_{K_R_EFF} + 0.23 \log q_{K_BA}$,

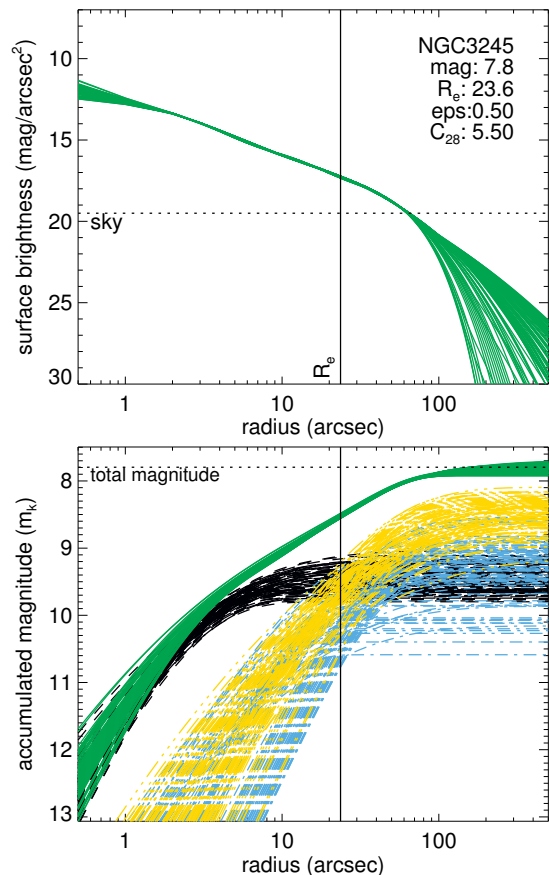


Figure 4. Example of the growth curve fit. The top panel shows the deconvolved surface brightness along the major axis for NGC3245. For each of the 100 fits, the outer Sérsic index n is changed from 0.5 to 4. Above the sky level (dotted line) the photometry is well constrained. Below the sky level, varying n forces the photometry to probe the largest extent of profiles with different slopes allowed by the data. The central region also shows scatter, due to degeneracy with the AGN point source included in the model. The half-light radius is shown as the vertical line. The bottom panel shows the curve-of-growth, radius versus enclosed light. Even though the surface brightness profile is not very well constrained at large radii, the enclosed mass is very well constrained, as the outer part below the sky level does not contain a significant amount of flux. The three Sérsic profiles of each iteration in Monte-Carlo fits are shown as the (dotted)-dashed lines. Multiple Sérsic fits are very degenerate, however the total flux is well constrained. The extrapolated total magnitude is shown as the dotted line. Identical figures for the other galaxies are available in a figure set.

in which $q_{K,BA}$ is the flattening of the galaxy in the XSC. Comparison with deeper photometry yields better results. The regression with the deep K-band photometry from Läscher et al. (2014a) is $m_K = 0.03 + 1.003m_{K,läscher}$ (where $m_{K,läscher}$ is the integrated magnitude inside the 24 mag/arcsec² isophote, as defined by Läscher et al. 2014a), which indicates a perfect match within the uncertainties. The work by Läscher et al. 2014a does not quote individual errors, nonetheless the inferred uncertainty of $\delta m_{24} = 0.05$ is consistent with their estimated systematic error. This indicates that the 2D growth curves on the 2MASS photometry is sufficiently accurate for the purpose of determining the black hole scaling relations and that photometry is not the limiting factor (see also Vika et al. 2012).

For reference, figure 5 also shows a comparison of the apparent magnitudes measured in K band with those measured in SDSS *i*-band from Beifiori et al. (2012) and with *Spitzer* 3.6 micron from Savorgnan & Graham (2016). It should be noted that comparisons between different bands suffer from differences in stellar populations and dust attenuation; even dust-free ellipticals have color gradients. In addition, total magnitudes from the literature are not derived using the growth-curve analysis adopted here. The *i*-band total magnitudes were derived using isophotal analysis and the 3.6 μ magnitudes were measured in the context of Bulge-Disk decompositions. While I find a significant scatter of ~ 0.3 dex in the colors, there is no systematic dependence on total luminosity, indicating that the 2MASS images are deep enough to measure the total flux for these objects.

2.3. Fitting linear regressions

Linear regressions can be fitted using various algorithms. The four most commonly used to measure BH scaling relations are those that have been tested by e.g. Park et al. (2012). In this work, I use the `mlinmixerr` and `linmixerr` routines by Kelly (2007). These routines use a Bayesian approach to multiple linear regression. The main reason for choosing this Gibbs sampler is that it includes the ability to incorporate upper-limits on the black hole masses and co-variance between the observables. Here the algorithm is used to find the coefficients of regressions of the form $Z = \alpha + \beta X + \gamma Y$ as well as the scatter ϵ around variable Z . In this work, the scatter is around the BH mass, except when applied to the galaxy Fundamental Plane in the next section, where it is on the σ_e variable. The mean and the standard deviation of the posterior distribution supplies the quoted measures of the best-fit values and 1σ uncertainties.

The regressions in this work are all log-linear regressions. Thus all the BH masses, luminosities, sizes, dispersions and their errors are converted to logarithmic units before fitting. The unit of Re is kiloparsec, while L_k is given in solar luminosities, σ_e is in km s⁻¹, and mass is in M_\odot .

The fitting algorithm allows for uncertainties on all parameters as well as for covariance between them. Uncertainties on the photometry and the spatially resolved BH masses are both affected by the distance uncertainty. Although the distance is not an explicit parameter of the regression, the error needs to be well-known and correctly propagated to the uncertainties of the other variables by combining them in quadrature. For most galaxies, the uncertainty on the BH mass is significantly bigger than the distance error. The velocity dispersion is not affected by distance errors, as the aperture in which it is measured (should) depend only on the apparent size of the galaxy. Luminosity, half-light radius and M_\bullet all depend on distances and thus cause (additional) covariance between parameters.

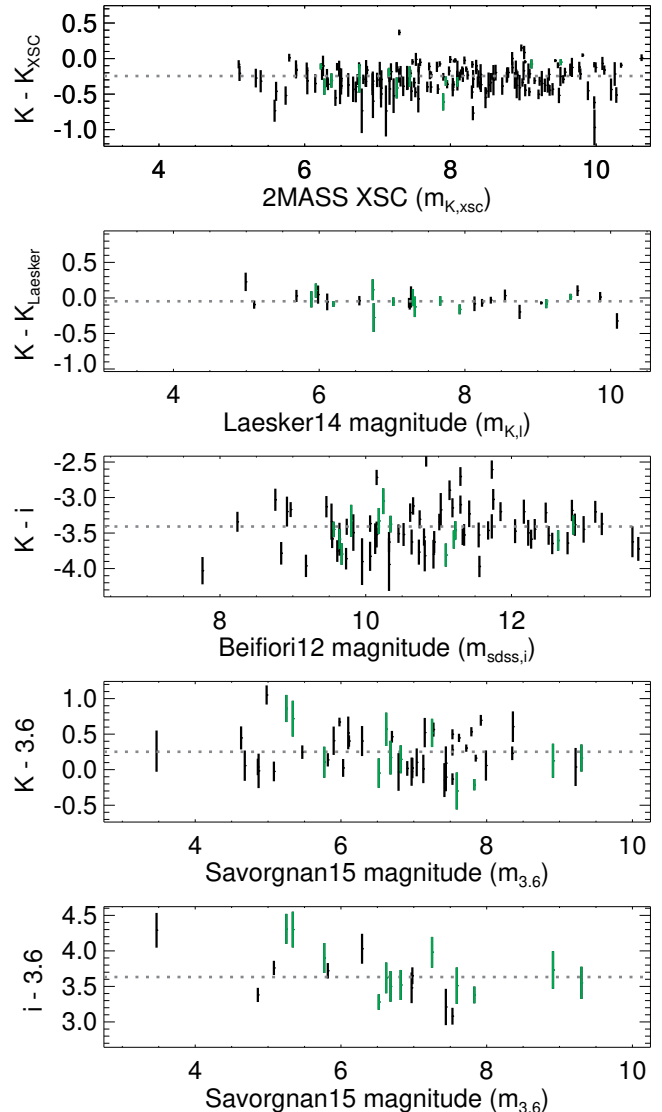


Figure 5. Comparison of the total apparent magnitudes with respect to other studies and bands. From top to bottom the comparison band becomes redder. The top shows the comparison between SDSS *i* band from Beifiori et al. (2012) derived using isophotal analysis. The middle panel shows the total magnitude derived from deep K-band using `galfit` from Läscher et al. (2014b). The bottom panel shows the comparison with *Spitzer* 3.6 micron from Savorgnan & Graham (2016). The range on the *x*- and *y*-axis is the same in all panels. Residuals are smallest when comparing identical K band, as is expected. Mean colors are $m_K - m_{K,läscher} = 0.05$, $m_K - m_i = -3.4$ and $m_K - m_{3.6} = 0.25$. While there is significant scatter (due to the different bands and methods), no systematic trend is seen as function of apparent magnitude. This indicates that the 2MASS images is deep enough to measure the total flux for these objects. The green objects are common to all samples.

The most significant covariance is between the luminosity (c.q. mass) and size, which is directly computed during the Monte-Carlo growth-curve fits. This includes the effect of the distance error onto the covariance. For the scaling relations fits in this paper, the other covariance terms are very small and are (assumed to be) negligible (Saglia et al. 2016).

2.4. Omitted Objects

All regressions in this paper are performed on the same set of 230 galaxies to ensure that they can be reliably compared against one another. Not all galaxies in the compilation are included in the fits. As previously mentioned, 32 galaxies are

excluded because of incomplete data (Table 3). (They lack either 2MASS growth curves (§2.2.1) or a velocity dispersion.) Another 15 galaxies are excluded from the fits because they are strong systematic outliers and one or more of their data are arguably suspect. Specifically, under the assumption that the scaling relations presented here are true, these 16 galaxies are outliers because:

- The literature dispersion is too high (NGC1300) or low (NGC2139, NGC5194, NGC4041) or has a unrealistically small error.
- Both NGC2139, NGC4636, NGC5018, NGC4699, NGC4826 and NGC4736 are significant outliers in the FP and BH-size-luminosity relation, possibly due to systematic uncertainties in their distances. The latter three BH masses come from unpublished literature (see Kormendy et al. 2011; Saglia et al. 2016).
- Both NGC1068 and NGC7469 are much too bright in K -band. They appear denser and brighter than the densest galaxies in the sample. Either their distance is in error (Yoshii et al. 2014) or there is significant additional flux from the starburst seen in these galaxies (Wilson et al. 1986).
- MRK110, MRK279 and NGC3156 have a bright AGN and its host galaxy is too faint for a robust growth curve with 2MASS.
- The surface brightness of NGC4395 is too low for a robust growth curve analysis with 2MASS. Based on optical photometry, the half-light radius is 1 kpc and the total stellar mass is $10^{8.9} M_{\odot}$ (den Brok et al. 2015; Reines & Volonteri 2015), which is consistent with their black hole mass and velocity dispersion estimates.

All of the above cases are systematically excluded from all fits considered in this study. However, for full disclosure, they are all still included in the figures but marked as ‘omitted’. Including (excluding) individual objects increases (decreases) the measured scatter, but does not significantly change the coefficients of the regressions. Previous studies often exclude more objects, which is why they typically find smaller scatter on their scaling relations. For example, <http://blackhole.berkeley.edu> lists 97 galaxies, of which 19 are labeled ‘complicated’.

3. THE GALAXY FUNDAMENTAL PLANE

The first step in the analysis is the construction of a Fundamental Plane for all the black hole host galaxies. The ETGs are well known to obey a tight Fundamental Plane. Spiral galaxies also obey dynamical scaling relations. Although they are not typically included in the Fundamental Plane, they too must obey the Virial Theorem as the underlying gravitational physics is the same. Applied to ETGs, the FP works so well because, inside the half light radius, the gravitating mass consists almost completely of stars; dark matter, the BH and non-homology are not dominant factors inside $1 R_e$ (see 5.2). In addition, the collision-less nature of stars makes them a good tracer of the second moment of the velocity tensor. The same is also true for star-forming disk galaxies. The dark matter fraction inside the half-light radius of a spiral galaxy is small, with the dark matter only becoming dominant at two disk scale lengths (Bershady et al. 2011; Courteau & Dutton 2015), which is equivalent

to $3.3 R_e$ for an exponential disk. The main complication for spirals is that the light more often (than in their early-type counterparts) traces a mixture of stellar populations of various ages and metallicities as well as star formation. This can be mitigated by using photometry in the infrared where changes in mass-to-light ratio are minimized (see also §5.2.1, Falcón-Barroso et al. 2011; Meidt et al. 2014; Norris et al. 2014a). The fit of a Fundamental Plane to large samples of heterogeneous galaxy types has already been successfully considered (Zaritsky et al. 2008; Falcón-Barroso et al. 2011; Bezanson et al. 2015).

As described below, the black hole host galaxies in the present sample, with uniform K -band photometry, do indeed follow the Fundamental Plane. In an effort to stay reminiscent of the Virial Theorem, I choose to consider the form $\sigma_e \propto L_k^{\alpha} R_e^{\beta}$. This has the benefit that 1) it has nearly the same variables as the canonical black hole scaling relations 2) the variables on both sides are (nearly) independent from one another and 3) the `mlinmixerr` routine only supports upper limits on the fitted variable, which will become relevant later.

The regression results in

$$\log\left(\frac{\sigma_e}{\text{km s}^{-1}}\right) = (2.11 \pm 0.01) + (0.71 \pm 0.03) \log\left(\frac{L_{\star}}{10^{11} L_{\odot}}\right) + (-0.72 \pm 0.05) \log\left(\frac{R_e}{5 \text{kpc}}\right). \quad (1)$$

The edge-on view of this plane is shown in figure 6. The intrinsic scatter is only ($\epsilon = 0.07 \pm 0.01$). (Note that there are a few outliers interpreted as bad data, see §2.4) and excluded from this and subsequent fits.) The scatter is very small, especially when compared to the black hole scaling relations for which the scatter is six times larger. Adding a concentration term, such as Sérsic n or C_{28} , improves the mass estimator by a small amount (e.g. Zaritsky et al. 2006; Courteau et al. 2007b; Taylor et al. 2010; Courteau et al. 2014), but such second order effects are outside the scope of the current paper.

The coefficients of the FP regression in eq. 1 are remarkably close to the Virial Theorem, yielding $L_k \propto R_e^{1.01} \sigma_e^{1.40}$. This corresponds to a ‘tilt’ with respect to the Virial Theorem by $R_e^{-0.01} \sigma_e^{0.60}$. Within the uncertainties, this tilt is solely in the σ_e direction. The half-light radius term is negligible, as also found by Cappellari et al. (2013b) for a sample of 260 early-type galaxies. The regression also provides a constraint on the covariance between the two exponents on L_k and R_e , implied to be quite strong and negative (-0.9). This suggests that the largest amount of freedom in the tilt is predominantly in the σ_e direction. Overall, the small tilt and the tightness of the FP provide strong indications that this Fundamental Plane is very close to the Virial Theorem. The K -band luminosity thus appears to be a very good proxy for the baryonic mass for these galaxies. Later in section 5.2.1 the tilt in the Fundamental Plane will be discussed and used to convert the total luminosity to total stellar mass.

From figure 6 it can be concluded that there is an empirical Fundamental Plane in the K -band that applies to all the black hole host galaxies with very little scatter. This plane holds equally well from the lowest mass $10^8 M_{\odot}$ dwarf galaxies to the $10^{13} M_{\odot}$ BCGs. The existence of this tight Fundamental Plane provides validation of the dataset, including the homo-

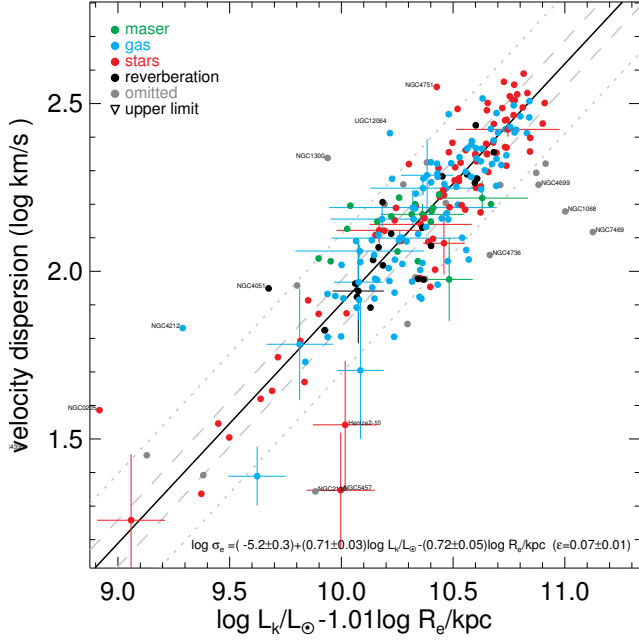


Figure 6. Galaxies lie on a remarkably tight Fundamental Plane with a scatter of $(\epsilon = 0.07 \pm 0.01)$ – 5 times smaller than the M_{\bullet} – σ relation. This demonstrates that the galaxy luminosity and size together are an extremely good proxy for the stellar velocity dispersion (see §3). Note that objects outlying the relation most likely have issues with their data and are not suspected to be true outliers of the Virial Theorem. Symbol shape is the same as in figure 1, while symbol color denotes the type of M_{\bullet} measurement (§2) performed for each host galaxy (although BH mass is not a fitted parameter). Note as well that the x-axis has the same units as in figure 7.

geneous photometry, the stellar velocity dispersion and the distances. In addition, since many of the galaxies probed here do not have a bulge, this suggests that σ_e is not intrinsically linked with the bulge mass but rather more directly to global photometric properties, as the strong correlation in figure 6 implies. Although bulge fraction might still be found to link with the Fundamental Plane parameters, the prominence of the bulge seems most likely to show a (partial) dependence on the concentration of the galaxy.

4. THE M_{\bullet} – σ AND HIGHER ORDER RELATIONS

Now that the Fundamental Plane of the host galaxies is established, this section focuses on the black hole scaling relations. The first is the relation between black hole mass and velocity dispersion. With the sample of black hole host galaxies defined in section 2.1, the resulting regression for the M_{\bullet} – σ relation is

$$\log \left(\frac{M_{\bullet}}{M_{\odot}} \right) = (8.32 \pm 0.04) + (5.35 \pm 0.23) \log \left(\frac{\sigma_e}{200 \text{ km s}^{-1}} \right), \quad (2)$$

which is shown in figure 1. This is quite similar to that found in previous studies, which is to be expected given that they consider the same galaxies. The regression is specifically consistent with McConnell & Ma (2013) and Saglia et al. (2016) but slightly steeper than Beifiori et al. (2012); Kormendy & Ho (2013). The intrinsic scatter around M_{\bullet} here, which is $(\epsilon = 0.49 \pm 0.03)$ is ~ 0.1 larger than found in previous work. This is primarily due to the increased sample size, which is twice as large as most previously studied samples and includes many more low mass objects. Note, though, that the scatter could of course be artificially reduced by selectively excluding the largest outliers, as is typical of previous results. The scatter

may also be sensitive to (small) differences in the adopted errors and in the fitting method, which varies between this and other analyses. The bayesian `linmixerr` fitting routine used here is more general and produces a larger scatter with respect to other methods (Park et al. 2012).

A tightening of the M_{\bullet} – σ relation might be possible with the introduction of a secondary photometric parameter, as considered by Saglia et al. (2016). That recent, exhaustive study explored several higher order regressions in detail and found only a minor improvement over the single variate M_{\bullet} – σ relation when including bulge parameters. Other searches integrating the photometry of the bulges have identified relations with much stronger dependence on R_e and a low exponent on σ_e such that $M_{\bullet} \propto \sigma_e^3 R_{bul}^{0.4}$ (e.g. Marconi & Hunt 2003; Aller & Richstone 2007; Hopkins et al. 2007b; Saglia et al. 2016). But none of these relations are (significantly) better than the M_{\bullet} – σ relation. Especially when considering the large systematic uncertainties inherent to the heterogeneous sample.

As tabulated in table 1, here I consider whether global host properties rather than bulge properties can serve as an additional tightening parameter and fit regressions between σ_e and either R_e , L_k or concentration C_{28} . None of these additional parameters yields a significant improvement, or even changes the slope on σ_e outside of the 1σ uncertainty. I thus conclude that the M_{\bullet} – σ is a universal relation spanning from the smallest to largest BH masses, is independent of galaxy type, and has no dependence on any additional global photometric parameter. This reaffirms the earlier conclusions of Gültekin et al. (2009a) and Beifiori et al. (2012) that the black hole scaling relation is driven solely by the velocity dispersion.

α	β	X	γ	Y	ϵ
-4.00 ± 0.51	5.35 ± 0.23	$\log \sigma_e$	–	–	(0.49 ± 0.03)
-3.99 ± 0.52	5.35 ± 0.24	$\log \sigma_e$	-0.01 ± 0.13	$\log R_e$	(0.49 ± 0.03)
-4.94 ± 0.96	5.07 ± 0.32	$\log \sigma_e$	0.14 ± 0.12	$\log L_k$	(0.49 ± 0.03)
-3.96 ± 0.51	5.10 ± 0.28	$\log \sigma_e$	0.10 ± 0.07	C_{28}	(0.49 ± 0.03)
-9.84 ± 1.11	1.60 ± 0.10	$\log M_{\bullet}$	–	–	(0.76 ± 0.05)
-11.06 ± 1.38	1.70 ± 0.12	$\log L_k$	–	–	(0.84 ± 0.05)
-30.47 ± 1.98	3.66 ± 0.19	$\log L_k$	-3.42 ± 0.26	$\log R_e$	(0.57 ± 0.04)
-22.58 ± 1.42	2.91 ± 0.14	$\log M_{\bullet}$	-2.77 ± 0.22	$\log R_e$	(0.52 ± 0.03)
-31.55 ± 1.92	3.78 ± 0.18	$\log L_k/R_e$	–	–	(0.57 ± 0.04)

Table 1

Black hole scaling relations based on parameter X and optionally a second parameter Y. The form of the regressions are $\log M_{\bullet} = \alpha + \beta X + \gamma Y$ with intrinsic scatter ϵ . Adding a second parameter does not improve the scatter, nor significantly change the coefficients on M_{\bullet} – σ relation.

5. UNIFICATION OF THE FUNDAMENTAL PLANE AND SUPER-MASSIVE BLACK HOLES MASSES

If the M_{\bullet} – σ relation (eq. (2)) obeyed by black holes does not depend on any additional parameters and the galaxies that host them follow the Fundamental Plane (eq. (1); with only a small tilt in the σ_e direction), then it follows that there is a black hole scaling relation in which σ_e can be replaced by (L_k/R_e) . This is indeed the case, as I show in this section.

5.1. Constraining σ and M_{\bullet} with galaxy luminosity & size

To demonstrate that, as expected from the Fundamental Plane, σ_e can be replaced by (L_k/R_e) in the M_{\bullet} – σ relation, I first show that there is a strong correlation between M_{\bullet} and (L_k/R_e) by fitting an independent regression. Then I show that this relation is consistent with the M_{\bullet} – σ relation. Figure 7 shows this independent fit for the BH–size–luminosity relation of the form

$$\begin{aligned} \log\left(\frac{M_\bullet}{M_\odot}\right) &= (7.37 \pm 0.06) \\ &+ (3.66 \pm 0.19) \log\left(\frac{L_\star}{10^{11}L_\odot}\right) \\ &+ (-3.42 \pm 0.26) \log\left(\frac{R_e}{5\text{kpc}}\right), \quad (3) \end{aligned}$$

with an intrinsic scatter of ($\varepsilon = 0.57 \pm 0.04$). Remarkably, the coefficients on the $\log L_k$ and $\log R_e$ terms are of the same magnitude even though they are independent variables of the fit. Moreover, as these coefficients are of opposite sign, when considered as exponents on L_k and R_e they imply that the ratio L_k/R_e is fundamentally well constrained, i.e. equation (3) implies $M_\bullet \propto (L_k/R_e)^{3.8}$. This would seem to lend credibility to the (L_k/R_e) identity, as it did for the FP in section 3. Imposing a 1D regression with $\log(L_k/R_e)$ as the sole variable yields a nearly identical coefficient, as tabulated in table 1, and with almost the same amount of scatter and uncertainty as equation (3). This form $M_\bullet \propto (L_k/R_e)^{3.8}$ has the advantage that it has one less free parameter and the covariance between L_k and R_e becomes implicit.

Most importantly, the regression given in equation (3) is equatable to the empirical M_\bullet – σ relation. With the help of the galaxy Fundamental Plane, eq. (1), it can be recast as

$$\log(M_\bullet) \propto \left(\frac{L_k^{3.66}}{R_e^{3.42}}\right) \approx (\sigma_e^{1.40})^{3.78} \propto \sigma_e^{5.29}, \quad (4)$$

which is consistent with the independently-derived $M_\bullet \propto \sigma_e^{5.4 \pm 0.2}$ from section 4. This shows that luminosity–size regression is, in fact, consistent with being a projection of the M_\bullet – σ relation. This consistency is also evident from the nearly identical x -axes shared by the galaxy Fundamental Plane in figure 6 and the $M_\bullet \propto (L_k/R_e)^{3.8}$ regression in figure 7. I conclude that this BH–size–luminosity relation is just another identity of M_\bullet – σ .

This was similarly found by Beifiori et al. (2012) – namely $M_\bullet \propto L_{i,\star}^{3.15 \pm 0.57} R_e^{-2.76 \pm 0.64}$ – albeit with larger uncertainties. In other studies, such as Barway & Kembhavi (2007) and Hopkins et al. (2007b), the focus was on (decomposed) photometry of bulges and hence similar coefficients are not found. As bulges lie on a narrow sequence in mass and size (the Kormendy relation, see §6), it can be difficult to robustly fit them with a plane.

Interestingly, whereas the Maser galaxies appear as slight outliers in the M_\bullet – σ relation (fig. 1, Greene et al. 2016) this is less pronounced in the BH–size–luminosity relation. Many of the objects that have BH mass upper limits in the literature are actually consistent with the BH–size–luminosity relation. It appears that the literature dispersions for many of these objects may be a little off; the Fundamental Plane also predicts a different dispersions (σ_e) for these objects (see also footnote 2).

5.2. Constraining σ and M_\bullet with galaxy mass & size

So far in this work I have considered only empirical scaling relations based on directly observable quantities, such as the total luminosity of the galaxy. However, the total stellar mass is a much more convenient basis for comparison with other works and theoretical predictions. The K -band luminosity is already a very good proxy for stellar mass, because variations in stellar mass-to-light ratios are strongly reduced in the (near-)infrared

bands compared to optical bands (Meidt et al. 2014; Norris et al. 2014a). Color information can generally be used to reliably estimate the mass-to-light ratio, but it is worth noting that dynamical and spectroscopic models both imply that the massive ellipticals have poorly understood IMF variations that are not manifest in broad band colors (Smith 2014).

5.2.1. Conversion to stellar mass

For the sake of simplicity, I use yet another scaling relation to estimate the mass-to-light ratio M_\star/L_k . Recent studies of the Fundamental Plane indicate that roughly 50-100 percent of its tilt is caused by variations of the stellar mass-to-light ratio (Cappellari et al. 2006, 2013a; Zaritsky et al. 2006; Bolton et al. 2008; Auger et al. 2010; Graves & Faber 2010; Falcón-Barroso et al. 2011) and the remainder due to non-homology, projection effects, the black hole and dark matter.⁶ Hence I adopt the average and assume that 75% of the tilt is solely caused by mass-to-light variations and that galaxies with a dispersion of 166 km s^{-1} have $1.0 M_\odot/L_{\odot,K}$ from Kormendy & Ho (2013). This directly yields $M_\star/L_K = 0.10 \sigma_e^{0.45}$. This factor, which is required only to convert L_k into M_\star , represents only a small change (less than a factor 2) in the mass-to-light ratio across the full range in σ_e probed by the galaxies in the sample.

Using this conversion, the Fundamental Plane can be converted into a virial mass estimator: $GM_\star = 9.5 \sigma_e^{1.85} R_e^{1.01}$. The slight (assumed) tilt is only in the velocity dispersion direction. This estimator and the ad hoc factor $\kappa = 9.5$ have been studied in detail in many other works (see Courteau et al. 2014 for a review). The value of κ found here is slightly higher than the value found by Cappellari (2016) due to the (assumed) offset of $\sigma_e^{-0.14}$ with respect to the Virial Theorem.

5.2.2. An independent regression in terms of galaxy mass

The BH–size–luminosity relation can be also re-fit with galaxy mass replacing K -band luminosity to yield

$$\begin{aligned} \log\left(\frac{M_\bullet}{M_\odot}\right) &= (7.48 \pm 0.05) \\ &+ (2.91 \pm 0.14) \log\left(\frac{M_\star}{10^{11}M_\odot}\right) \\ &+ (-2.77 \pm 0.22) \log\left(\frac{R_e}{5\text{kpc}}\right), \quad (5) \end{aligned}$$

(The scatter is slightly lower than the original due to inclusion of the σ_e in the definition mass-to-light ratio used to convert L_k to galaxy mass. See table 1.) Just like the BH–size–luminosity relation, this mass relation can be expressed in terms of only two constants instead of three, as $M_\bullet \propto (M_\star/R_e)^{2.9}$, given the curious fact that the tilt of the Fundamental Plane is in the same direction as the M_\bullet – σ relation. This form is especially

⁶ The super-massive black hole itself could be a contributor to the tilt of the FP. The BH mass fraction is typically much less than 1% and does typically not contribute significantly to the global observables of a galaxy. The main exception is M60UCD1 in which the BH mass fraction is bigger than 10%. This stripped object is not included in the fits, because it is not resolved in the 2MASS imaging (Seth et al. 2014). In second place is NGC4486B (7%) which is regularly considered to be an outlier (Gültekin et al. 2009b). In third place is NGC1277 (2%). The latter two objects are included in the FP and the M_\bullet – σ relation in this work and are not outliers. However, simple numerical tests do show that the BH can contribute to the dispersion in extreme cases. Isotropic Jeans models (Watkins et al. 2013) of NGC1277 and M87 (without dark matter) with and without a BH show a change in σ_e of about nine percent. The BH could thus be a partial contributor to the tilt in the fundamental plane.

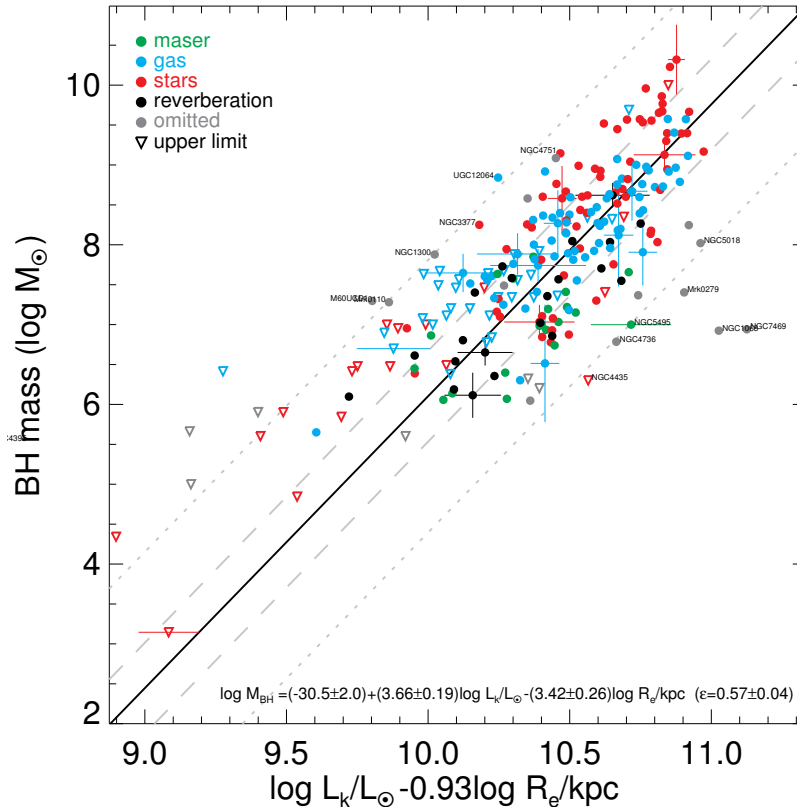


Figure 7. The BH–size–luminosity relation – shown here – has a similar amount of scatter as the M_{\bullet} – σ relation. The black-hole–plane tilts in the same direction as the galaxy Fundamental Plane (fig. 6). Hence the relation shown here is just a reprojection of the M_{\bullet} – σ relation. The coefficients of this regression have nearly the same ratio as the Fundamental Plane, which is why the x -axis here is very similar to the one in figure 6. The symbols are the same as in figure 1.

useful when comparing to the predictions of semi-analytical models and to, e.g., the sub-grid physics in hydro-dynamical simulations of galaxies and the accretion histories of the super-massive black holes.

It should be emphasized that the main conclusion of this paper — $M_{\bullet} \propto \sigma_e^{5.4} \equiv M_{\bullet} \propto (L_k/R_e)^{3.8}$ — is an empirical relation and is completely independent of the choice for the mass-to-light ratio conversion.

6. BLACK HOLES IN RELATION TO THE SIZES AND MASSES OF DISKS AND BULGES

Different subsets of galaxies occupy different regions of the Fundamental Plane. The distribution of the present sample of black hole host galaxies in mass and size is shown in figure 8. (Another view is shown in figure 2.) Overplotted in figure 8 are the mass–size relations of the ETGs and the disks galaxies. For other variations of this plot see Janz et al. (2016) for the distribution of quiescent galaxies or see van der Wel et al. (2014) for the size evolution of galaxies as function of redshift. The ETGs lie on a narrow sequence (Chen et al. 2010) and the disk galaxies lie on a relation with a larger scatter (Courteau et al. 2007a). Where the two populations intersect is typically where lenticular galaxies are located. In the next two subsections, the projections of these two populations will be discussed separately.

As revealed in this study, the black hole scaling relations are all linked together through the Fundamental Plane. The predicted BH mass expected from the $M_{\bullet} \propto (L_k/R_e)^{3.8}$ relation is indicated relative to the galaxy population by contours in figure 8. Compared to previous compilations (e.g. Shankar

et al. 2016), the significantly expanded sample of 230 objects considered here is much more representative of the galaxy population.⁷ Still, the host galaxies in the present sample are not very homogeneous across the global galaxy population. Some regions are over-sampled while others are very sparse. The L_{\star} dense ellipticals, for one, are over-represented (Yu & Tremaine 2002; van den Bosch et al. 2015; Shankar et al. 2016), whereas the low mass galaxies are under-sampled. More leverage on the black hole scaling relation can be created by targeting host galaxies in the under-sampled regions. The lowest mass galaxies are underrepresented because of the resolution limit of $0.1''$ of today’s optical and near-infrared telescopes (van den Bosch et al. 2015)

6.1. Ellipticals and Bulges

Black holes are well known to exhibit a strong correlation with bulge mass, but at first glance the $M_{\bullet} \propto (L_k/R_e)^{3.8}$ and the canonical $M_{\bullet} \propto M_{bul}^1$ relation appear incompatible. As described below, however, this is just a projection effect.

Consider, to start, that ellipticals (and their bulges) obey a tight relation between their size and mass (e.g. Kormendy et al. 2009). This reprojects into the Faber-Jackson ($L \propto \sigma^4$, 1976) and Kormendy (1977) relations using the Fundamental Plane. The same power-law followed by ellipticals is also followed by compact ellipticals and UCDs (e.g. Norris et al. 2014b), all systems with a Bulge-to-Total ratio that is close to unity (i.e. almost all of their mass is in a bulge). In this

⁷ The Shankar et al. (2016) sample was published during the review of this paper.

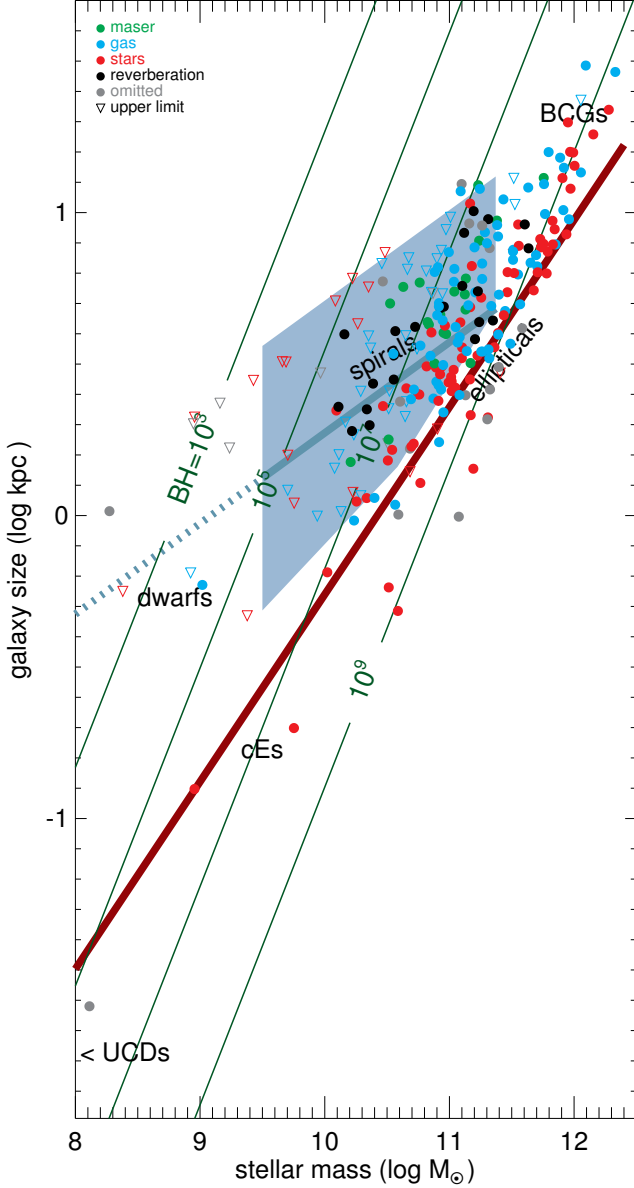


Figure 8. Distribution of the sizes and total luminosities of the sample with respect to the spiral and elliptical galaxies. The ellipticals fall on the Kormendy relation, shown as the red line. The late-type galaxies also follow a much wider mass–size relation, shown in blue. At $10^{11} M_{\odot}$ the two families intersect. A 1D projection of these two relations is shown in figure 2. The BH–size–mass relation is plotted as green contours, indicating the expected black hole mass. This plots highlights the uneven sampling of the black hole host galaxy distribution which mostly reflects the limits imposed by the spatial resolutions of current telescopes. Color coding of the symbols is the same as in figure 1.

case, $M_{\star} \sim M_{bul}$ and, as such, the relation shown in red in Figure 8 for the densest galaxies, can be translated into a relation in terms of bulge mass. Figure 8 specifically shows the mass–size relation from deep K-band photometry from Läscher et al. (2014a). Their 34 bulge-dominated galaxies yield an independently derived relation:

$$\log(R_e/\text{kpc}) = -7.09 + 0.68(L_k/L_{\odot}) \quad (6)$$

All of the galaxies close to this (red) line in figure 8 are bulge-dominated (e.g. Savorgnan & Graham 2016) and thus have Bulge-to-Total ratios of nearly 1 so that $M_{\star} \sim M_{bul}$. Equation (6) can thus be combined with (4) to produce the black

hole mass projection for these galaxies:

$$\log(M_{\bullet}/M_{\odot}) = -4.98 + 1.21 \log(M_{\star}/M_{\odot}), \quad (7)$$

which is shown in figure 2. This projection is consistent with other previous K-band M_{\bullet} – M_{bul} relations (Kormendy & Ho 2013; Graham & Scott 2013; Läscher et al. 2014b). It appears that the canonical $M_{\bullet} \propto M_{bul}^1$ relation is just the projection of the M_{\bullet} – σ relation onto the Kormendy relation. Is this a coincidence? Or is it regulated by physics? The principal question is what causes the slope of the quiescent galaxy mass–size relations, which is unchanging with redshift (van der Wel et al. 2014).

Although BH mass can be cast in terms of bulge mass, as in eq. 7, the M_{\bullet} – σ relation, and its proxy $M_{\bullet} \propto (L_k/R_e)^{3.8}$, should be preferred over the $M_{\bullet} \propto M_{bul}^1$ as they are more universally applicable and do not require a bulge definition of any kind. Both apply to all stellar systems and are completely independent of galaxy type and bulge-to-total fraction. Thus they also work for completely bulge-less galaxies. In contrast, the M_{\bullet} – M_{bul} relation only applies to galaxies with a classical bulge. In the case of pseudo-bulges, the bulge mass is already well known to provide a less accurate prediction of black hole mass than in the M_{\bullet} – σ relation (Saglia et al. 2016; Savorgnan et al. 2016). Furthermore, as shown in section 4, the M_{\bullet} – σ relation does not appear to be improved upon by, e.g. adding the C_{28} concentration parameter.

There is no existing 2D relation that includes bulge properties that has been found to be significantly better than the M_{\bullet} – σ relation. It therefore seems plausible that there is, in fact, no causal link between the bulge and black hole mass. Of course, revealing such a link, if one exists, is complicated by the difficulty of estimating the bulge fraction, which depends strongly on the definition of bulge used and is strongly degenerate when measured with multiple Sérsic functions. Even so, the scaling relations all appear to be tightly linked. For example, the $M_{\bullet} \propto (\sqrt{M_{bul}}\sigma_e^2)^{1.09}$ from Saglia et al. (2016) for classical bulges (see also Hopkins et al. 2007a,c; Aller & Richstone 2007; Feoli et al. 2011) directly maps onto the canonical $M_{\bullet} \propto M_{bul}^1$ relation when combined with the M_{\bullet} – σ relation. For (pseudo-)bulges, which form a separate Fundamental Plane different from the total mass Fundamental Plane, a (crude) mapping between the total galaxy FP and the bulge FP also arguably exists, given that this plane still uses the same σ_e (Sani et al. 2011; Saglia et al. 2016). The multitude of secular processes thought to make (pseudo-)bulges grow in disk galaxies could somehow correlate with SMBH accretion, leading to a correlation between BH and pseudo-bulge mass. However, this process, if it exists, does not seem to have the same vector as σ on the Fundamental Plane.

Despite the link between different scaling relations, the M_{\bullet} – σ and $M_{\bullet} \propto (L_k/R_e)^{3.8}$ relations do not necessarily always imply the same BH masses as the M_{\bullet} – M_{bul} relation. A prime example is the case of the black holes in the Brightest Cluster galaxies (BCGs), which are the most massive galaxies at the tip of the luminosity function. When extrapolating from the lower mass ellipticals, these galaxies curve away from the Kormendy relation such that they have relatively large size for their mass (Lauer et al. 2007a). As a result, their velocity dispersions hit a ceiling at 400 km s^{-1} . The M_{\bullet} – σ relation thus predicts a lower BH mass than the M_{\bullet} – M_{bul} relation. (Note that massive galaxies are well represented in this compilation, with 31 galaxies more massive than M87, suggesting that the M_{\bullet} – σ relation as measured here remains valid at the high mass end.) Likewise, the $M_{\bullet} \propto (M_{\star}/R_e)^{2.9}$ predicts that the biggest black holes reside

in the highest dispersion galaxies and not in the most luminous. Lower mass ($10^{11.2} M_{\odot}$) galaxies with high dispersions are more numerous and likely host the biggest black holes (Lauer et al. 2007b).

6.2. Disk and spiral galaxies

Disk galaxies also follow a mass–size relation, although it is not as tight as the Kormendy relation for bulge dominated ETGs. For example, using the transformation from section 2.2.1, the size–luminosity relation from Courteau et al. (2007a) based on the 2MASS XSC of spirals with $L_k > 10^{9.5} M_{\odot}$ can be converted to

$$\log(R_e/\text{kpc}) = -3.39 + 0.36(L_k/L_{\odot}) \quad (8)$$

This is shown as the blue line in figure 8. The shaded blue area denotes the 2σ scatter as measured by Courteau et al. (2007a). (Note that the spiral galaxies in the present sample are reasonably sampled down to a mass of $10^{9.5} M_{\odot}$, but the sampling becomes very sparse at the low mass end.) The mass–size relation for disks can then be combined with equation (4) to predict a 1D black hole mass relation. The prediction is shown as a blue line in figure 2 and can be expressed as

$$\log(M_{\bullet}/M_{\odot}) = -14.36 + 2.02\log(M_{\star}/M_{\odot}) \quad (9)$$

This relation intersects with the ellipticals because the two mass–size relations also intersect. This is unlike the parallel relation for AGNs from Reines & Volonteri (2015), perhaps suggesting that the AGN host galaxies follow a different mass–size relation than the spirals.

Low mass dwarf galaxies also host black holes. This is supported by evidence of active nuclei in their centers (e.g. Greene & Ho 2007; Reines et al. 2011, 2013; Sartori et al. 2015). The dwarfs may very well be the best way to study the seed formation of SMBHs in the local universe. The smallest SMBH is found in RGG118, which has a black hole mass of $10^{4.7} M_{\odot}$ (Baldassare et al. 2015). The existence of a seed mass for SMBH formation would imply that the BH scaling relations need to truncate somewhere, in contrast to equation (9), which predicts that BH masses do not suddenly truncate. One way to test whether such a truncation exists is to confirm that galaxies below a certain mass do not host AGNs. For example, if the SMBH seed mass is $10^4 M_{\odot}$, then eq. (9) indicates that there would be no AGNs in disk galaxies with masses below $10^{8.5} M_{\odot}$.

6.3. Globular clusters and Ultra-Compact dwarfs

There has been much recent effort to measure the black hole masses in dense stellar systems, including Globular Clusters and Ultra-Compact Dwarfs (UCDs). These systems are not included in this compilation as they have very different formation histories than normal galaxies. Their black hole masses are also much more uncertain. However, in this section, I briefly compare their BH mass estimates to the BH–size–luminosity relation.

Globular clusters are not quite dense enough to lie on the Kormendy relation (Misgeld et al. 2011). According to the $M_{\bullet} \propto (L_k/R_e)^{3.8}$ relation, given their sizes and masses these systems should not host intermediate mass BHs over $1000 M_{\odot}$. I speculate that Globular Clusters do not host SMBHs at all. This is consistent with non-detections at radio and X-ray wavelengths (Strader et al. 2012; Miller-Jones et al. 2012; Haggard et al. 2013) and upper-limits from stellar dynamics

(van den Bosch et al. 2006; Lanzoni et al. 2013; den Brok et al. 2014; Kamann et al. 2014, 2016), but in contrast with the black hole mass detections from (Lützgendorf et al. 2011, 2013, 2015). Yet other observational evidence (Lanzoni et al. 2013; Bianchini et al. 2015) as well as arguments from dynamical analyses (anisotropy and mass-to-light variations van den Bosch et al. 2006; Kamann et al. 2016; Zocchi et al. 2016) suggest that this mass could be considered an upper limit. The appendix A contains a compilation of BH mass measurements in GCs. Some of the Ultra Compact Dwarfs (UCDs) are dense enough to host SMBHs (Mieske et al. 2013). This is indeed the case for M60-UCD1 (Seth et al. 2014), but does not appear to be the case for NGC4546-UCD1 and UCD3 (Norris et al. 2015; Frank et al. 2011). Other UCD’s are stripped galaxies that still host the original SMBH of their progenitor (Norris et al. 2014b). The exact delineation between UCDs and globular clusters is not yet clear and many objects lie in between. For instance, it is not clear whether M31’s G1 (Gebhardt et al. 2005) and ω Centauri (van de Ven et al. 2006; Noyola et al. 2010; van der Marel & Anderson 2010) are stripped galaxies, like the UCDs, or like the highest mass globular clusters (without a black hole). Given their stellar masses and sizes they could be either.

7. DISCUSSION & CONCLUSIONS

In this paper I examine the nature of the scaling relations linking black holes with their host galaxies. For this empirical study I combine 230 black hole masses and host galaxy velocity dispersions from the literature with new K -band photometry derived uniformly for all galaxies from 2D growth curves. With these data I confirm that BH host galaxies obey two empirical dynamical scaling relations: the Fundamental Plane $L_k \propto R_e^{1.01} \sigma_e^{1.40}$ and the $M_{\bullet} \propto \sigma_e^{5.4}$. The Fundamental Plane, traversing the space defined by galaxy mass, size and velocity dispersion, is the tighter of the two relations. The 1D scaling relations obeyed individually by the dwarf, spiral and elliptical galaxy populations are thus recognizable as projections of the different distributions of each class of object on the FP.

The fact that the Fundamental Plane applies to all galaxy types, including those with and without (pseudo-)bulges, has important implications for the mutual relevance of the relations that link BH mass to either the velocity dispersion σ_e or to bulge mass. Since the global photometry of bulge-less galaxies is a very good predictor of σ_e , the velocity dispersion by itself is arguably not a (direct) tracer of the bulge mass, as it is often invoked. (Bulge mass correlates with the global host galaxy properties but can not be predicted solely by σ_e .) Furthermore, only the M_{\bullet} – σ relation is relevant for the bulge-less galaxies that host super-massive black holes, like NGC4395 (and does indeed predict black hole masses consistent with observations). I therefore argue that the M_{\bullet} – σ relation is the optimum universal relation. Even if the physics of bulge formation and black hole growth are linked, it thus appears that bulge properties are not an optimal predictor of black hole mass, particularly when a galaxy lacks a detectable bulge.

The Fundamental Plane and the M_{\bullet} – σ relation together constitute a basis that can define other scaling relations applicable to galaxies of all types. In particular, I reveal the existence of the BH–size–luminosity relation $M_{\bullet} \propto (L_k/R_e)^{3.8}$, which has the same amount of scatter as the M_{\bullet} – σ relation. This scaling relation is completely expected from the combination of the M_{\bullet} – σ relation and the Fundamental Plane. Thus, the BH–size–luminosity relation is just another identity of $M_{\bullet} \propto \sigma_e^{5.4}$, as

I demonstrate in section 6.1, where I show that the projection of the Kormendy relation for bulges is consistent with the canonical black-hole–bulge-mass relation of $M_{\bullet} \propto M_{bul}^1$.

The BH–size–luminosity relation can be recast in terms of stellar mass, adopting a conversion between luminosity and stellar mass. In section 5.2.1 I adopt a simple mass-to-light ratio estimator based on the slight tilt observed in the Fundamental Plane with respect to the Virial Theorem. The BH–size–luminosity relation becomes $M_{\bullet} \propto (M_{\star}/R_e)^{2.9}$ and the total mass of a galaxy can be approximated with $GM_{\star} = 9.5\sigma_e^{1.85}R_e^{1.01}$.

The new BH–size–luminosity relation (and its cousin, the BH–size–mass relation) serves particularly well when the stellar velocity dispersion of the host galaxy is not known, such as in cases when the galaxy is faint (e.g. $z > 0$ or low surface brightness), or when the velocity dispersion is below the instrumental resolution. The existence of the relation also offers a unique perspective on why total galaxy mass (or proxy L_k) by itself is not a good predictor of BH mass (fig. 2, Reines & Volonteri 2015), as has also been reproduced by recent cosmological galaxy simulations with SMBHs (e.g. Anglés-Alcázar et al. 2013; Schaye et al. 2015; Steinborn et al. 2015; Volonteri et al. 2016). If the M_{\bullet} – σ relation is indeed universal, the number density of SMBHs (Lauer et al. 2007b; Shankar et al. 2009; Kelly & Merloni 2012) would seem best derived from the galaxy velocity dispersion function (Sheth et al. 2003; Bezanson et al. 2012), rather than the galaxy mass function.

At larger distances ($z > 0$), where it becomes much harder to accurately measure σ_e , the BH–size–mass relation is ideal. It remains unclear, though, whether today’s M_{\bullet} – σ relation also holds at earlier times. Strong evolution is implied by the increase in galaxy size within the quiescent galaxy population with redshift (van der Wel et al. 2014), but there are hints that individual galaxies may still evolve such that the M_{\bullet} – σ relation stays intact at each epoch. For example, the relic galaxies NGC1271, NGC1277, b19 and MRK1216 (Walsh et al. 2015, 2016; Läsker et al. 2013; Yıldırım et al. 2015) all formed at $z > 2$ and have evolved passively ever since (Ferré-Mateu et al. 2015). These galaxies are much smaller than most present day ETGs and host extremely big black holes (Walsh et al. 2015, 2016). Even though they formed a long time ago, they are still consistent with the black hole scaling relations today.

The scaling relations presented in this work can be improved in several ways. First, homogeneity in the measurements should be pursued. While the photometry all comes from the same instrument, the stellar velocity dispersions and black hole masses for the galaxies in the present sample are measured with a variety of techniques and instrumentation and are highly heterogeneous in quality. Velocity dispersions measured from IFUs have been shown to significantly decrease the scatter in the FP (Cappellari et al. 2013a), but such measurements are not available for most of these black hole host galaxies. The most homogenous spectroscopic dataset of BH hosts comes from the long slit observations from the HETMGs. Even with a homogenous dataset one must still insure that dispersions are defined and measured consistently. Different definitions of, and alternative units for, σ will directly change the coefficients of the M_{\bullet} – σ relation and can change the scatter. In this work, I have preferred measurements of σ_e , as they are the most widely available and the closest to the dispersion as expressed

in the Virial Theorem. However, alternative definitions are also possible (§2.1) and might possibly yield a more fundamental M_{\bullet} – σ relation. For example, the definition of the dispersion advanced by McConnell & Ma (2013) specifically excludes the region around the BH, to decouple the measured dispersion from the influence of the BH.

Another improvement can be made by using a stellar dynamics to forward model projection effects (Bellovary et al. 2014) and derive dynamical mass-to-light ratios and the dark matter content with a homogenous data set and dynamical methods. The non-uniformity of the black hole mass measurements themselves must also be alleviated. The commonly used set of techniques for black hole mass measurements all probe different types of host galaxies, but ideally a significant sample is studied under the same conditions and with the same consistently applied technique. This includes adopting the same set of assumptions in stellar dynamical models, which have significantly changed over the last two decades (e.g. triaxiality, dark matter haloes, and systematics, see Kormendy & Ho 2013). Cross-calibrations of BH mass measurement techniques and uniformity across larger samples of BH masses is highly desirable for future progress (van den Bosch et al. 2016).

Although this paper describes several empirical black hole scaling relations, it does not examine their causality. The fact that the M_{\bullet} – σ relation appears to be universal and applies to all galaxy types would seem to hint at some form of feedback process between the SMBH and the host galaxy. Many of the most common theories for black hole–galaxy coevolution link black hole and bulge growth together. Other theories involving direct black hole feedback link the black hole mass to σ^4 or σ^5 , based on energy or momentum driven winds (King 2003; Fabian 1999; Silk & Rees 1998). The functional form found here, $M_{\bullet} \propto \sigma_e^{5.4 \pm 0.2}$, is closest to the momentum driven theories. Even if these theories are correct, the merging history must play an important role in establishing the M_{\bullet} –host galaxy relation (Peng 2007; Jahnke & Macciò 2011) through the virtue of the central limit theorem

ACKNOWLEDGMENTS

I am grateful for comments on the manuscript from the anonymous referee, the manuscript editor Sharon E. M. van der Wel, Stephane Courteau, Nathalie Ouellette, Lisa Steinborn, Glenn van de Ven, Akin Yıldırım, Tim de Zeeuw and, to Nadine Neumayer for insisting the figures should use stellar mass, instead of luminosity.

This publication makes use of data products from the Two Micron All Sky Survey, which is a joint project of the University of Massachusetts and the Infrared Processing and Analysis Center/California Institute of Technology, funded by the National Aeronautics and Space Administration and the National Science Foundation.

The work depended greatly on the public databases, [HyperLeda](#) (Paturel et al. 1997), NASA’s Astrophysics Data System and the NASA/IPAC Extragalactic Database (NED), which is operated by the Jet Propulsion Laboratory, California Institute of Technology, under contract with the National Aeronautics and Space Administration. This research has made use of NASA’s Astrophysics Data System.

Name	Distance	M_{\odot}	σ_e	L_k	R_e	covar.	C_{28}	AGN	method	ref.
(1)	Mpc	$\log(M_{\odot})$	$\log(\text{km s}^{-1})$	$\log(L_{\odot})$	$\log(\text{kpc})$	L_k-R_e	(8)	$\log(L_{\odot})$	(10)	(11)
3C120	141.4±14.1	7.73±0.15	2.21±0.05	11.20±0.09	1.00±0.06	0.05	3.8±0.2	11.39±0.00	reverb	Kollatschny et al. (2014)
3C390.3	240.3±24.0	8.62±0.16	2.44±0.03	11.25±0.10	0.64±0.09	0.14	3.9±0.8	11.26±0.04	reverb	Dietrich et al. (2012)
A1836BCG	152.4±8.4	9.57±0.06	2.46±0.02	11.75±0.06	0.89±0.06	0.04	4.9±0.5	-	gas	Dalla Bontà et al. (2009)
A3565BCG	49.2±3.6	9.11±0.07	2.51±0.02	11.83±0.07	0.98±0.06	0.04	5.3±0.2	-	gas	Dalla Bontà et al. (2009)
Ark120	140.1±14.0	8.05±0.17	2.28±0.02	11.20±0.09	0.74±0.07	0.05	3.9±0.4	11.53±0.00	reverb	Doroshenko et al. (2008)
Arp151	90.3±9.0	6.65±0.16	2.07±0.01	10.62±0.09	0.45±0.13	0.10	10.9±3.3	-	reverb	Bentz et al. (2010)
Circinus	2.8±0.5	6.06±0.10	2.20±0.05	10.22±0.12	0.18±0.13	0.09	6.7±0.6	-	maser	Greenhill et al. (2003)
CygnusA	257.1±25.7	9.41±0.13	2.43±0.02	12.24±0.10	1.46±0.08	0.05	4.4±0.4	-	gas	Tadhunter et al. (2003)
ESO558-009	102.5±10.2	7.22±0.03	2.23±0.05	11.13±0.10	0.68±0.13	0.09	5.6±0.7	10.10±0.09	maser	Greene et al. (2016)
Fairall9	201.4±20.1	8.27±0.21	2.35±0.08	11.57±0.09	0.88±0.07	0.07	4.1±0.7	11.42±0.02	reverb	Peterson et al. (2004); van den Bosch et al. (2015)
Henize2-10	9.0±0.9	0.00 ^{+7.00} _{-0.00}	1.54±0.19	9.68±0.10	-0.33±0.10	0.06	5.1±0.7	-	star	Nguyen et al. (2014)
IC0342	3.7±0.4	6.41 ^{+0.29} _{-6.41}	1.78±0.17	10.65±0.10	0.83±0.11	0.13	3.4±0.2	-	gas	Beifiori et al. (2012)
IC1459	28.9±3.7	9.39±0.08	2.53±0.02	11.64±0.11	0.80±0.08	0.05	5.9±0.3	-	star	Cappellari et al. (2002)
IC1481	89.9±9.0	7.15±0.13	1.98±0.12	10.99±0.09	0.50±0.06	0.06	4.4±0.5	9.73±0.12	maser	Huré et al. (2011); van den Bosch et al. (2015)
IC2560	41.8±4.2	7.64±0.05	2.15±0.03	11.26±0.10	1.09±0.10	0.05	4.5±0.5	9.60±0.07	maser	Greene et al. (2016)
IC3639	44.8±4.5	7.01 ^{+0.35} _{-7.01}	1.96±0.02	10.76±0.09	0.33±0.05	0.07	3.8±0.5	9.71±0.13	gas	Beifiori et al. (2012)
J0437+2456	66.0±6.6	6.45±0.03	2.04±0.05	10.61±0.08	0.70±0.05	0.04	3.0±0.4	9.57±0.03	maser	Greene et al. (2016)
Mrk0050	100.3±10.0	7.40±0.18	2.03±0.06	10.44±0.08	0.30±0.06	0.07	3.2±0.8	9.93±0.03	reverb	Barth et al. (2011b)
Mrk0079	95.0±9.5	7.58±0.23	2.11±0.04	11.17±0.09	0.93±0.06	0.04	3.2±0.3	10.99±0.00	reverb	Peterson et al. (2004)
Mrk0202	90.0±9.0	6.11±0.28	1.89±0.02	10.48±0.10	0.35±0.09	0.10	5.8±2.0	9.48±0.21	reverb	Bentz et al. (2010)
Mrk0509	147.3±14.7	8.03±0.15	2.26±0.03	11.19±0.10	0.58±0.09	0.09	4.1±0.7	11.54±0.01	reverb	Peterson et al. (2004)
Mrk0590	113.0±11.3	7.55±0.18	2.28±0.01	11.58±0.09	0.96±0.06	0.05	5.1±0.4	11.14±0.01	reverb	Peterson et al. (2004)
Mrk0817	134.7±13.5	7.57±0.18	2.08±0.05	11.17±0.08	0.76±0.05	0.05	3.6±0.6	11.23±0.00	reverb	Denney et al. (2010)
Mrk1216	94.0±9.4	9.30 ^{+0.70} _{-9.30}	2.49±0.01	11.29±0.09	0.47±0.07	0.06	6.6±2.2	-	star	Yildirim et al. (2015)
Mrk1310	83.8±8.4	6.19±0.19	1.92±0.03	10.35±0.10	0.28±0.08	0.06	2.8±0.6	10.02±0.01	reverb	Bentz et al. (2010)
NGC0193	49.7±5.0	8.40±0.32	2.27±0.04	11.24±0.08	0.83±0.07	0.05	5.9±0.3	-	gas	Beifiori et al. (2012)
NGC0205	0.7±0.1	0.00 ^{+4.34} _{-0.00}	1.59±0.07	8.66±0.11	-0.25±0.08	0.05	3.4±0.5	-	star	Valluri et al. (2005)
NGC0221	0.8±0.0	6.39±0.19	1.87±0.02	9.11±0.04	-0.90±0.04	0.02	5.0±0.3	-	star	van den Bosch & de Zeeuw (2010)
NGC0289	17.1±1.7	7.38 ^{+0.30} _{-7.38}	2.03±0.05	10.60±0.08	0.35±0.04	0.04	3.0±0.2	-	gas	Beifiori et al. (2012)
NGC0307	52.8±5.7	8.60±0.06	2.31±0.01	10.95±0.08	0.44±0.07	0.06	6.5±0.6	-	stars	Saglia et al. (2016)
NGC0315	57.7±5.8	8.92±0.31	2.49±0.04	11.79±0.08	1.01±0.05	0.05	4.9±0.2	-	gas	Beifiori et al. (2012)
NGC0383	59.2±5.9	8.76±0.32	2.38±0.03	11.69±0.11	1.09±0.13	0.07	6.1±0.4	-	gas	Beifiori et al. (2012)
NGC0404	3.1±0.3	5.65±0.25	1.39±0.09	9.39±0.10	-0.23±0.09	0.05	4.7±0.3	-	gas	Seth et al. (2010)
NGC0428	16.1±1.6	4.48 ^{+0.37} _{-4.48}	1.50±0.07	10.01±0.09	0.51±0.06	0.04	3.4±0.3	-	star	Neumayer & Walcher (2012)
NGC0524	24.2±2.2	8.94±0.05	2.37±0.02	11.29±0.08	0.56±0.07	0.04	4.7±0.4	-	star	Krajnović et al. (2009)
NGC0541	63.7±6.4	8.59±0.34	2.28±0.01	11.36±0.10	0.92±0.09	0.06	6.1±0.3	-	gas	Beifiori et al. (2012)
NGC0598	0.8±0.1	0.00 ^{+3.15} _{-0.00}	1.26±0.20	9.39±0.12	0.32±0.10	0.11	2.8±0.4	6.59±0.06	star	Gebhardt et al. (2001); Merritt et al. (2001)
NGC0613	15.4±1.5	7.60±0.35	2.09±0.07	10.97±0.12	0.82±0.11	0.06	4.7±0.3	-	gas	Beifiori et al. (2012)
NGC0741	65.7±6.6	8.67±0.37	2.37±0.02	11.82±0.09	1.18±0.07	0.05	5.5±0.3	-	gas	Beifiori et al. (2012)
NGC0788	47.9±4.8	7.92±0.28	2.10±0.06	11.14±0.09	0.59±0.09	0.05	4.6±0.6	-	gas	Beifiori et al. (2012)
NGC0821	23.4±1.8	8.22±0.21	2.32±0.02	11.14±0.08	0.82±0.09	0.05	5.9±0.3	-	star	Schulze & Gebhardt (2011)
NGC1023	10.8±0.8	7.62±0.05	2.22±0.02	10.94±0.07	0.49±0.10	0.06	5.9±0.4	-	star	Bower et al. (2001)
NGC1042	18.2±1.8	4.40 ^{+2.08} _{-4.40}	1.64±0.07	10.48±0.09	0.78±0.06	0.05	2.8±0.5	8.03±0.21	star	Neumayer & Walcher (2012)
NGC1052	18.1±1.8	8.24±0.29	2.28±0.01	10.92±0.08	0.34±0.05	0.05	5.4±0.3	-	gas	Beifiori et al. (2012)
NGC1097	14.5±1.5	8.14±0.09	2.29±0.01	11.18±0.10	0.74±0.12	0.08	6.1±0.4	-	CO	Onishi et al. (2015)
NGC1194	58.0±6.3	7.85±0.05	2.17±0.07	11.06±0.09	0.74±0.06	0.05	5.8±0.4	9.54±1.89	maser	Kuo et al. (2011)
NGC1271	84.0±8.4	9.53±0.06	2.45±0.01	11.07±0.08	0.33±0.07	0.07	9.1±4.0	-	star	Walsh et al. (2015)
NGC1275	70.0±7.0	8.98±0.20	2.39±0.05	11.84±0.08	1.15±0.05	0.05	4.9±0.2	-	gas	Scharwächter et al. (2013); van den Bosch et al. (2015)
NGC1277	71.0±7.1	9.67±0.15	2.50±0.01	11.07±0.08	0.15±0.07	0.07	7.8±3.2	-	star	Walsh et al. (2016)
NGC1316	18.6±0.6	8.18±0.25	2.35±0.02	11.91±0.06	1.20±0.13	0.07	6.0±0.3	-	star	Nowak et al. (2008)
NGC1320	49.1±4.9	6.74±0.16	2.15±0.05	11.01±0.09	0.60±0.08	0.07	5.2±0.4	9.21±3.27	maser	Greene et al. (2016)
NGC1332	22.3±1.9	8.83±0.04	2.52±0.02	11.31±0.08	0.68±0.12	0.06	6.9±0.6	-	CO	Barth et al. (2016)
NGC1358	48.2±4.8	8.37±0.32	2.23±0.05	11.28±0.11	0.94±0.12	0.07	5.9±0.5	-	gas	Beifiori et al. (2012)
NGC1374	19.2±0.7	8.76±0.06	2.31±0.02	10.67±0.03	0.24±0.03	0.02	5.2±0.3	-	star	Rusli et al. (2013)
NGC1386	16.1±1.6	6.07±0.29	2.22±0.02	10.51±0.08	0.25±0.06	0.05	5.5±0.3	8.66±1.93	maser	Braatz et al. (1997)
NGC1398	24.8±4.1	8.03±0.08	2.37±0.01	11.66±0.15	0.91±0.11	0.08	5.6±0.4	-	stars	Saglia et al. (2016)
NGC1399	20.9±0.7	8.94±0.31	2.53±0.02	11.54±0.05	0.74±0.09	0.05	5.6±0.4	-	star	Gebhardt et al. (2007); Houghton et al. (2006)
NGC1407	28.0±3.4	9.65±0.08	2.45±0.02	11.72±0.12	0.97±0.11	0.08	5.4±0.5	-	star	Rusli et al. (2013)
NGC1428	20.7±2.1	0.00 ^{+7.00} _{-0.00}	1.91±0.02	9.89±0.09	0.04±0.06	0.05	3.8±0.3	-	star	Lyubenova et al. (2013)
NGC1493	11.4±1.1	5.40 ^{+0.51} _{-5.40}	1.55±0.07	9.96±0.12	0.51±0.09	0.07	3.1±0.6	-	star	Neumayer & Walcher (2012)
NGC1497	75.3±7.5	8.63±0.19	2.39±0.04	11.32±0.08	0.73±0.05	0.05	5.4±0.4	-	gas	Beifiori et al. (2012)
NGC1550	51.6±5.6	9.57±0.07	2.48±0.02	11.32±0.10	0.66±0.08	0.05	5.8±0.4	-	star	Rusli et al. (2013)
NGC1600	64.0±6.4	10.23±0.04	2.47±0.02	11.86±0.08	1.08±0.05	0.04	4.9±0.2	-	star	Thomas et al. (2016)
NGC1667	56.1±5.6	8.20±0.23	2.24±0.07	11.32±0.10	0.69±0.08	0.05	3.9±0.6	-	gas	Beifiori et al. (2012)
NGC1961	48.6±4.9	8.29±0.34	2.34±0.08	11.74±0.09	1.20±0.07	0.05	5.5±0.4	-	gas	Beifiori et al. (2012)
NGC2110	29.1±2.9	8.12±0.64	2.30±0.05	11.04±0.08	0.40±0.06	0.05	5.6±0.4	-	gas	Beifiori et al. (2012)

Table continues on next page.

Name	Distance	M_{\bullet}	σ_e	L_k	R_e	covar.	C_{28}	AGN	method	ref.
(1)	Mpc	$\log(M_{\odot})$	$\log(\text{km s}^{-1})$	$\log(L_{\odot})$	$\log(\text{kpc})$	L_k-R_e	(8)	$\log(L_{\odot})$	(10)	(11)
NGC2179	35.8±3.6	8.31±0.23	2.19±0.03	10.86±0.10	0.53±0.08	0.05	5.9±0.4	-	gas	Beifiori et al. (2012)
NGC2273	29.5±1.9	6.93±0.04	2.16±0.05	10.98±0.07	0.60±0.09	0.05	5.8±0.5	-	maser	Kuo et al. (2011)
NGC2329	72.3±7.2	8.18±0.18	2.34±0.03	11.46±0.10	0.84±0.08	0.06	5.4±0.3	-	gas	Beifiori et al. (2012)
NGC2549	12.7±1.6	7.16±0.37	2.15±0.02	10.29±0.10	0.05±0.05	0.05	5.4±0.2	-	star	Krajinović et al. (2009)
NGC2685	12.5±1.3	6.59 ^{+0.41} _{-6.59}	2.02±0.02	10.20±0.09	0.20±0.08	0.05	5.1±0.3	-	gas	Beifiori et al. (2012)
NGC2748	23.4±8.2	7.65±0.24	2.06±0.02	10.62±0.25	0.53±0.14	0.13	4.2±0.3	-	gas	Atkinson et al. (2005)
NGC2778	23.4±2.3	7.16 ^{+0.30} _{-7.16}	2.12±0.02	10.27±0.08	0.08±0.06	0.05	5.1±0.4	-	star	Schulze & Gebhardt (2011)
NGC2787	7.4±1.2	7.61±0.09	2.28±0.02	10.21±0.13	-0.02±0.07	0.06	4.9±0.3	-	gas	Sarzi et al. (2001)
NGC2892	86.2±8.6	8.43±0.11	2.47±0.03	11.54±0.08	0.83±0.07	0.05	5.2±0.4	-	gas	Beifiori et al. (2012)
NGC2903	10.4±1.0	7.06 ^{+0.28} _{-7.06}	1.97±0.06	11.06±0.12	0.73±0.11	0.04	3.3±0.3	-	gas	Beifiori et al. (2012)
NGC2960	67.1±7.1	7.03±0.05	2.18±0.02	11.14±0.09	0.73±0.08	0.08	5.7±0.3	10.02±0.11	maser	Kuo et al. (2011); van den Bosch et al. (2015)
NGC2964	19.7±2.0	6.73 ^{+0.61} _{-6.73}	1.97±0.09	10.63±0.08	0.41±0.05	0.05	4.0±0.4	-	gas	Beifiori et al. (2012)
NGC2974	21.5±2.4	8.23±0.09	2.36±0.02	11.04±0.09	0.55±0.07	0.06	5.8±0.4	-	stars	Cappellari et al. (2008)
NGC3021	22.4±2.2	7.26 ^{+0.30} _{-7.26}	1.70±0.20	10.40±0.09	0.31±0.06	0.04	3.6±0.3	-	gas	Beifiori et al. (2012)
NGC3031	3.6±0.1	7.81±0.13	2.15±0.02	10.93±0.08	0.44±0.11	0.04	5.0±0.3	-	gas	Devereux et al. (2003)
NGC3078	32.8±3.3	7.91±0.42	2.32±0.03	11.27±0.09	0.55±0.07	0.05	5.6±0.4	9.57±0.04	gas	Beifiori et al. (2012)
NGC3079	15.9±1.2	6.40±0.05	2.16±0.02	10.86±0.07	0.63±0.05	0.03	5.4±0.4	-	maser	Trotter et al. (1998); Yamauchi et al. (2004); Kondratko et al. (2005)
NGC3081	33.5±3.4	7.20±0.30	2.09±0.03	10.96±0.11	0.66±0.13	0.06	5.4±0.6	-	gas	Beifiori et al. (2012)
NGC3091	51.2±8.3	9.56±0.07	2.49±0.02	11.62±0.12	0.89±0.09	0.07	5.7±0.4	-	star	Rusli et al. (2013)
NGC3115	9.5±0.4	8.95±0.09	2.36±0.02	10.98±0.04	0.42±0.06	0.03	5.4±0.3	-	star	Emsellem et al. (1999)
NGC3227	23.8±2.6	7.32±0.23	2.12±0.04	11.21±0.13	1.03±0.14	0.06	4.9±0.4	9.51±0.12	star	Davies et al. (2006)
NGC3245	21.4±2.0	8.38±0.11	2.25±0.02	10.86±0.09	0.39±0.05	0.05	5.5±0.3	9.26±0.15	gas	Barth et al. (2001)
NGC3310	17.4±1.7	6.70 ^{+0.92} _{-6.70}	1.92±0.02	10.42±0.09	0.07±0.08	0.05	4.7±0.8	-	gas	Pastorini et al. (2007)
NGC3351	9.3±0.9	6.52 ^{+0.26} _{-6.52}	1.97±0.07	10.76±0.10	0.59±0.11	0.06	4.9±0.4	-	gas	Beifiori et al. (2012)
NGC3368	10.4±1.0	6.88±0.08	2.08±0.09	10.95±0.07	0.49±0.06	0.05	5.7±0.4	-	star	Nowak et al. (2010)
NGC3377	11.0±0.5	8.25±0.25	2.11±0.02	10.52±0.06	0.36±0.11	0.06	5.9±0.4	-	star	Schulze & Gebhardt (2011)
NGC3379	10.7±0.5	8.62±0.11	2.27±0.02	11.01±0.06	0.48±0.09	0.05	6.3±0.5	-	star	van den Bosch & de Zeeuw (2010)
NGC3384	11.5±0.7	7.03±0.21	2.14±0.02	10.85±0.09	0.49±0.21	0.14	7.1±0.7	-	star	Schulze & Gebhardt (2011)
NGC3393	49.2±8.2	7.20±0.33	2.17±0.03	11.15±0.15	0.78±0.11	0.09	5.8±0.4	9.52±0.14	maser	Kondratko et al. (2008)
NGC3414	25.2±2.7	8.40±0.07	2.28±0.02	10.99±0.11	0.46±0.08	0.05	5.5±0.3	-	stars	Cappellari et al. (2008)
NGC3423	14.6±1.5	5.18 ^{+0.67} _{-5.18}	1.62±0.07	10.35±0.09	0.71±0.07	0.04	3.6±0.2	-	star	Neumayer & Walcher (2012)
NGC3489	12.1±0.8	6.78±0.05	2.01±0.02	10.60±0.07	0.18±0.08	0.06	5.9±0.5	9.15±0.05	star	Nowak et al. (2010)
NGC3585	20.5±1.7	8.52±0.13	2.33±0.02	11.42±0.07	0.80±0.07	0.04	5.7±0.3	-	star	Gültekin et al. (2009a)
NGC3607	22.6±1.8	8.14±0.16	2.32±0.02	11.35±0.07	0.60±0.09	0.05	5.8±0.5	-	star	Gültekin et al. (2009a)
NGC3608	22.8±1.5	8.67±0.10	2.23±0.02	10.92±0.07	0.47±0.06	0.04	5.5±0.3	-	star	Schulze & Gebhardt (2011)
NGC3621	6.6±0.7	6.00 ^{+0.48} _{-6.00}	1.79±0.03	10.46±0.10	0.63±0.11	0.06	4.9±0.6	-	star	Barth et al. (2009)
NGC3627	10.1±1.1	6.93±0.05	2.09±0.01	11.02±0.09	0.63±0.07	0.05	4.0±0.4	-	stars	Saglia et al. (2016)
NGC3642	21.6±2.2	7.42 ^{+0.04} _{-7.42}	1.97±0.11	10.35±0.10	0.27±0.06	0.05	4.5±0.3	-	gas	Beifiori et al. (2012)
NGC3665	34.7±6.7	8.76±0.09	2.34±0.02	11.50±0.15	0.80±0.09	0.08	5.4±0.3	-	CO	Onishi et al. (2016)
NGC3675	12.4±1.2	7.26 ^{+0.29} _{-7.26}	2.02±0.02	10.83±0.09	0.55±0.06	0.05	4.0±0.2	-	gas	Beifiori et al. (2012)
NGC3706	46.0±4.6	9.77±0.06	2.51±0.01	11.58±0.08	0.80±0.05	0.04	5.8±0.4	-	star	Gültekin et al. (2014)
NGC3783	41.7±4.2	7.36±0.19	1.98±0.05	11.06±0.10	0.69±0.06	0.05	3.6±0.4	10.58±0.01	reverb	Onken & Peterson (2002)
NGC3801	46.3±4.6	8.28±0.31	2.32±0.04	11.22±0.09	0.78±0.09	0.06	5.5±0.4	-	gas	Beifiori et al. (2012)
NGC3842	92.2±10.6	9.96±0.14	2.44±0.02	11.81±0.11	1.11±0.07	0.06	5.4±0.2	-	star	McConnell et al. (2011a)
NGC3862	84.6±8.5	8.41±0.37	2.32±0.03	11.59±0.09	1.08±0.10	0.07	6.5±0.3	-	gas	Beifiori et al. (2012)
NGC3923	20.9±2.7	9.45±0.12	2.35±0.02	11.50±0.11	0.89±0.10	0.06	5.1±0.4	-	stars	Saglia et al. (2016)
NGC3945	19.5±2.0	6.94 ^{+0.46} _{-6.94}	2.25±0.02	10.89±0.09	0.29±0.07	0.05	4.8±0.4	-	star	Gültekin et al. (2009a)
NGC3953	15.4±1.5	7.33±0.29	2.11±0.01	11.05±0.10	0.87±0.09	0.05	4.7±0.4	-	gas	Beifiori et al. (2012)
NGC3982	15.9±1.6	6.95 ^{+0.26} _{-6.95}	1.89±0.01	10.23±0.09	0.16±0.06	0.05	3.2±0.4	-	gas	Beifiori et al. (2012)
NGC3992	15.3±1.5	7.51±0.28	2.09±0.06	11.15±0.12	1.07±0.13	0.06	4.3±0.5	-	gas	Beifiori et al. (2012)
NGC3998	14.3±1.3	8.93±0.05	2.35±0.02	10.71±0.07	0.11±0.06	0.05	5.6±0.3	9.15±0.27	star	Walsh et al. (2012)
NGC4026	13.4±1.7	8.26±0.12	2.19±0.02	10.55±0.11	0.22±0.07	0.07	6.0±0.3	-	star	Gültekin et al. (2009a)
NGC4036	19.0±1.9	7.89±0.36	2.26±0.02	10.90±0.09	0.43±0.06	0.04	5.0±0.3	-	gas	Beifiori et al. (2012)
NGC4051	10.0±1.0	6.10±0.25	1.95±0.01	10.28±0.08	0.60±0.04	0.04	3.5±0.2	9.28±0.01	reverb	Denney et al. (2009)
NGC4088	11.9±1.2	6.79 ^{+0.29} _{-6.79}	1.93±0.02	10.50±0.08	0.55±0.04	0.04	3.2±0.1	-	gas	Beifiori et al. (2012)
NGC4143	14.8±1.5	7.92±0.36	2.25±0.02	10.55±0.08	0.04±0.05	0.05	5.3±0.4	-	gas	Beifiori et al. (2012)
NGC4150	12.8±1.3	5.94 ^{+0.44} _{-5.94}	1.91±0.02	10.08±0.10	-0.00±0.06	0.05	5.7±0.4	-	gas	Beifiori et al. (2012)
NGC4151	20.0±2.8	7.81±0.08	1.98±0.01	10.96±0.13	0.60±0.12	0.08	7.1±0.3	10.23±0.03	star	Onken et al. (2014)
NGC4203	14.1±1.4	7.82±0.26	2.11±0.02	10.76±0.11	0.42±0.13	0.07	5.8±0.4	-	gas	Beifiori et al. (2012)
NGC4212	3.2±0.3	5.99 ^{+0.42} _{-5.99}	1.83±0.02	9.10±0.09	-0.19±0.05	0.04	3.1±0.4	-	gas	Beifiori et al. (2012)
NGC4245	14.6±1.5	7.19 ^{+0.48} _{-7.19}	1.92±0.02	10.42±0.10	0.41±0.09	0.06	5.1±0.3	-	gas	Beifiori et al. (2012)
NGC4253	55.4±5.5	6.80±0.17	1.94±0.16	10.69±0.10	0.61±0.06	0.05	2.9±0.5	10.53±0.00	reverb	Bentz et al. (2010)
NGC4258	7.3±0.5	7.58±0.03	2.06±0.04	10.90±0.08	0.64±0.08	0.03	4.1±0.3	8.53±0.07	maser	Herrnstein et al. (2005)
NGC4261	32.4±2.8	8.72±0.10	2.42±0.02	11.60±0.09	0.86±0.12	0.06	5.5±0.5	-	gas	Ferrarese et al. (1996)
NGC4278	15.0±1.5	7.96±0.27	2.33±0.02	10.87±0.09	0.24±0.09	0.07	5.4±0.6	-	gas	Beifiori et al. (2012)
NGC4291	26.6±3.9	8.99±0.16	2.38±0.02	10.95±0.13	0.44±0.11	0.08	6.8±0.5	-	star	Schulze & Gebhardt (2011)
NGC4303	17.9±1.8	6.51±0.74	1.92±0.02	11.17±0.12	0.81±0.11	0.05	3.9±0.7	-	gas	Pastorini et al. (2007)
NGC4314	15.5±1.5	6.91 ^{+0.30} _{-6.91}	2.03±0.01	10.90±0.11	0.81±0.12	0.06	5.2±0.4	-	gas	Beifiori et al. (2012)

Table continues on next page.

Name	Distance	M_{\bullet}	σ_e	L_k	R_e	covar.	C_{28}	AGN	method	ref.
(1)	Mpc	$\log(M_{\odot})$	$\log(\text{km s}^{-1})$	$\log(L_{\odot})$	$\log(\text{kpc})$	L_k-R_e	(8)	$\log(L_{\odot})$	(10)	(11)
NGC4321	14.2±1.4	6.67 ^{+0.17} _{-6.67}	1.92±0.02	11.14±0.11	0.98±0.13	0.08	4.2±0.7	-	gas	Beifiori et al. (2012)
NGC4335	59.1±5.9	8.39±0.31	2.41±0.01	11.30±0.09	0.60±0.07	0.05	5.8±0.5	-	gas	Beifiori et al. (2012)
NGC4342	22.9±1.4	8.66±0.19	2.38±0.02	10.44±0.05	-0.24±0.06	0.04	8.6±3.6	-	star	Cretton & van den Bosch (1999)
NGC4350	17.0±1.7	8.58±0.41	2.24±0.02	10.69±0.09	0.23±0.07	0.05	6.0±0.4	-	star	Pignatelli et al. (2001)
NGC4371	16.9±1.5	6.84±0.07	2.16±0.02	10.78±0.08	0.40±0.05	0.04	4.7±0.3	-	stars	Saglia et al. (2016)
NGC4374	18.5±0.6	8.97±0.05	2.41±0.02	11.40±0.03	0.57±0.03	0.02	5.0±0.2	-	gas	Walsh et al. (2010)
NGC4382	17.9±1.8	7.11 ^{+1.24} _{-7.11}	2.25±0.02	11.50±0.09	0.86±0.08	0.05	4.8±0.5	-	star	Gültekin et al. (2011)
NGC4388	16.5±1.6	6.86±0.04	2.03±0.03	10.72±0.08	0.75±0.08	0.05	5.2±0.5	8.71±0.05	maser	Kuo et al. (2011)
NGC4429	18.2±1.8	7.85±0.35	2.25±0.02	11.42±0.15	1.04±0.18	0.06	5.2±0.4	-	gas	Beifiori et al. (2012)
NGC4435	17.0±1.7	0.00 ^{+6.30} _{-0.00}	2.18±0.02	10.70±0.09	0.14±0.05	0.05	5.2±0.3	-	star	Coccatto et al. (2006)
NGC4450	28.3±2.8	8.06 ^{+0.28} _{-8.06}	2.03±0.06	11.60±0.11	1.11±0.11	0.06	4.7±0.5	-	gas	Beifiori et al. (2012)
NGC4459	16.0±0.5	7.84±0.09	2.20±0.02	10.94±0.04	0.42±0.06	0.03	5.8±0.3	-	gas	Sarzi et al. (2001)
NGC4472	17.1±0.6	9.40±0.04	2.40±0.02	11.75±0.07	0.89±0.11	0.04	5.2±0.6	-	star	Walsh et al. (2013)
NGC4473	15.2±0.5	7.95±0.24	2.27±0.02	10.89±0.03	0.38±0.05	0.03	5.8±0.3	-	star	Schulze & Gebhardt (2011)
NGC4477	20.8±2.1	7.55±0.30	2.17±0.02	11.17±0.11	0.69±0.10	0.06	5.1±0.4	-	gas	Beifiori et al. (2012)
NGC4486	16.7±0.6	9.58±0.10	2.42±0.02	11.61±0.05	0.82±0.07	0.03	5.7±0.6	7.57±4.13	gas	Walsh et al. (2013)
NGC4486A	16.0±0.5	7.10±0.15	2.09±0.02	10.08±0.05	-0.19±0.06	0.03	4.9±0.7	-	star	Nowak et al. (2007)
NGC4486B	16.5±0.6	8.60±0.02	2.23±0.02	9.75±0.05	-0.70±0.12	0.10	4.8±2.7	-	star	Saglia et al. (2016)
NGC4501	16.5±1.1	7.30±0.08	2.20±0.01	11.27±0.07	0.72±0.04	0.03	3.5±0.2	9.23±0.07	stars	Saglia et al. (2016)
NGC4507	47.0±4.7	7.18±0.35	2.16±0.02	11.08±0.09	0.62±0.06	0.04	4.1±0.3	10.38±0.02	gas	Beifiori et al. (2012)
NGC4526	16.4±1.8	8.65±0.12	2.32±0.02	11.22±0.09	0.54±0.10	0.07	5.6±0.6	-	gas	Davis et al. (2013)
NGC4548	17.9±1.8	7.25±0.29	2.16±0.04	11.27±0.16	1.08±0.17	0.07	4.2±0.5	-	gas	Beifiori et al. (2012)
NGC4552	15.3±1.0	8.70±0.05	2.35±0.02	11.11±0.06	0.45±0.07	0.05	6.3±0.4	-	stars	Cappellari et al. (2008)
NGC4564	15.9±0.5	7.95±0.12	2.19±0.02	10.67±0.04	0.42±0.06	0.03	6.5±0.3	-	star	Schulze & Gebhardt (2011)
NGC4579	23.0±2.3	7.96 ^{+0.36} _{-7.96}	2.04±0.06	11.61±0.12	1.03±0.13	0.07	4.9±0.6	-	gas	Beifiori et al. (2012)
NGC4593	38.5±3.9	6.86±0.21	2.13±0.02	11.35±0.09	0.98±0.09	0.06	5.6±0.3	10.28±0.04	reverberb	Barth et al. (2013)
NGC4594	9.9±0.8	8.82±0.05	2.38±0.02	11.39±0.08	0.74±0.08	0.04	4.2±0.2	-	star	Jarrel et al. (2011)
NGC4596	16.5±6.2	7.89±0.26	2.10±0.02	10.97±0.26	0.70±0.16	0.14	5.3±0.3	-	gas	Sarzi et al. (2001)
NGC4621	18.3±3.0	8.60±0.09	2.30±0.02	11.19±0.12	0.53±0.06	0.06	5.2±0.2	-	stars	Cappellari et al. (2008)
NGC4649	16.5±0.6	9.67±0.10	2.43±0.02	11.66±0.06	0.90±0.10	0.05	5.8±0.5	-	star	Shen & Gebhardt (2010)
NGC4697	12.5±0.4	8.31±0.11	2.23±0.02	11.08±0.05	0.64±0.07	0.03	4.9±0.3	-	star	Schulze & Gebhardt (2011)
NGC4698	16.4±1.6	7.76±0.16	2.09±0.03	10.82±0.10	0.56±0.08	0.05	5.0±0.2	-	gas	Beifiori et al. (2012)
NGC4742	15.7±1.6	7.10±0.15	1.95±0.02	10.46±0.09	0.06±0.11	0.08	7.8±1.0	-	star	Tremaine et al. (2002)
NGC4748	62.7±6.3	6.36±0.26	2.02±0.05	10.82±0.09	0.62±0.06	0.04	3.4±0.3	10.30±0.01	reverberb	Bentz et al. (2010)
NGC4751	26.9±2.9	9.15±0.06	2.55±0.02	10.95±0.09	0.52±0.07	0.05	6.4±0.4	-	star	Rusli et al. (2013)
NGC4800	12.5±1.3	7.02 ^{+0.53} _{-7.02}	2.01±0.01	10.23±0.08	0.01±0.05	0.04	4.2±0.2	-	gas	Beifiori et al. (2012)
NGC4889	102.0±5.2	10.32±0.44	2.56±0.02	12.13±0.05	1.34±0.05	0.03	5.6±0.2	-	star	McConnell et al. (2011a)
NGC4945	3.7±0.4	6.14±0.18	2.13±0.02	10.80±0.12	0.77±0.12	0.08	3.9±0.4	-	maser	Greenhill et al. (1997)
NGC5005	14.6±1.5	8.27±0.23	2.30±0.02	11.10±0.09	0.54±0.06	0.04	5.0±0.2	-	gas	Beifiori et al. (2012)
NGC5055	8.7±0.9	8.92±0.10	2.00±0.02	11.13±0.10	0.77±0.09	0.05	4.7±0.5	-	gas	Blais-Ouellette et al. (2004)
NGC5077	38.7±8.4	8.93±0.27	2.35±0.02	11.26±0.16	0.52±0.08	0.08	5.1±0.3	-	gas	de Francesco et al. (2008)
NGC5127	62.5±6.3	8.27±0.41	2.29±0.11	11.35±0.09	0.96±0.07	0.05	5.4±0.3	-	gas	Beifiori et al. (2012)
NGC5128	3.6±0.2	7.76±0.08	2.18±0.02	11.04±0.06	0.41±0.06	0.03	4.9±0.4	-	star	Cappellari et al. (2009)
NGC5248	17.9±1.8	6.30±0.38	2.10±0.04	10.97±0.09	0.69±0.06	0.05	4.7±0.2	8.86±0.06	gas	Beifiori et al. (2012)
NGC5252	103.7±10.4	9.07±0.34	2.28±0.02	11.49±0.09	0.88±0.06	0.05	5.2±0.3	-	gas	Capetti et al. (2005)
NGC5273	15.5±1.5	6.61±0.27	1.82±0.02	10.29±0.09	0.36±0.07	0.05	4.1±0.2	7.49±3.18	reverberb	Bentz et al. (2014); van den Bosch et al. (2015)
NGC5283	34.5±3.5	7.41±0.33	2.13±0.04	10.44±0.08	0.06±0.05	0.06	5.3±0.7	-	gas	Beifiori et al. (2012)
NGC5328	64.1±7.0	9.67±0.16	2.52±0.02	11.71±0.09	0.94±0.06	0.05	6.0±0.3	-	star	Rusli et al. (2013)
NGC5347	32.3±3.2	7.21 ^{+0.42} _{-7.21}	1.80±0.08	10.54±0.09	0.59±0.07	0.05	5.2±0.3	-	gas	Beifiori et al. (2012)
NGC5419	56.2±6.1	9.86±0.14	2.57±0.01	12.00±0.09	1.26±0.07	0.05	5.5±0.2	-	stars	Saglia et al. (2016)
NGC5427	36.3±3.6	7.58 ^{+0.30} _{-7.58}	1.80±0.08	11.12±0.13	0.88±0.12	0.05	4.2±0.5	-	gas	Beifiori et al. (2012)
NGC5457	7.0±0.7	6.41 ^{+0.08} _{-6.41}	1.35±0.17	10.87±0.13	0.87±0.08	0.07	3.5±0.4	6.93±2.60	star	Kormendy et al. (2010)
NGC5490	65.2±6.5	8.73±0.35	2.41±0.04	11.48±0.09	0.70±0.07	0.05	6.0±0.4	-	gas	Beifiori et al. (2012)
NGC5495	126.3±11.6	7.00±0.05	2.22±0.05	11.76±0.14	1.11±0.15	0.15	3.8±1.9	-	maser	Greene et al. (2016)
NGC5516	58.4±6.3	9.52±0.06	2.48±0.04	11.83±0.09	1.30±0.09	0.06	6.3±0.2	-	star	Rusli et al. (2013)
NGC5548	73.6±7.4	7.70±0.13	2.29±0.03	11.21±0.09	0.64±0.06	0.06	5.2±0.6	10.85±0.03	reverberb	Kovačević et al. (2014)
NGC5576	25.7±1.7	8.44±0.13	2.19±0.02	11.18±0.06	0.69±0.07	0.04	6.7±0.3	-	star	Gültekin et al. (2009a)
NGC5643	17.4±1.7	7.05 ^{+0.59} _{-7.05}	1.95±0.01	11.09±0.12	0.94±0.13	0.06	3.8±0.8	-	gas	Beifiori et al. (2012)
NGC5695	54.6±5.5	8.00±0.32	2.16±0.01	10.97±0.10	0.64±0.08	0.04	4.6±0.4	-	gas	Beifiori et al. (2012)
NGC5728	37.6±3.8	8.05±0.29	2.28±0.09	11.28±0.10	0.90±0.08	0.05	6.0±0.3	-	gas	Beifiori et al. (2012)
NGC5765B	113.0±11.3	7.66±0.03	2.20±0.05	11.18±0.08	0.50±0.06	0.06	3.6±0.5	10.15±0.04	maser	Gao et al. (2016)
NGC5813	32.2±2.7	8.85±0.06	2.32±0.02	11.50±0.08	0.96±0.07	0.04	5.5±0.3	-	stars	Cappellari et al. (2008)
NGC5845	25.9±4.1	8.69±0.16	2.36±0.02	10.53±0.13	-0.31±0.10	0.09	5.2±1.2	-	star	Schulze & Gebhardt (2011)
NGC5846	24.9±2.3	9.04±0.06	2.35±0.02	11.46±0.09	0.80±0.10	0.06	5.0±0.5	-	stars	Cappellari et al. (2008)
NGC5879	10.6±1.1	6.62 ^{+0.28} _{-6.62}	1.73±0.06	9.92±0.09	0.08±0.06	0.05	4.5±0.4	-	gas	Beifiori et al. (2012)
NGC5921	20.5±2.0	7.07 ^{+0.42} _{-7.07}	1.93±0.05	10.79±0.12	0.81±0.11	0.05	4.3±0.5	-	gas	Beifiori et al. (2012)
NGC6086	138.0±11.5	9.57±0.17	2.50±0.02	11.87±0.08	1.20±0.08	0.06	6.2±0.4	-	star	McConnell et al. (2011b)
NGC6240(S)	105.0±10.5	9.17±0.21	2.44±0.07	11.84±0.09	0.93±0.08	0.05	7.1±1.0	-	star	Medling et al. (2011)
NGC6251	108.4±9.0	8.79±0.16	2.46±0.02	11.95±0.07	1.13±0.07	0.05	5.8±0.3	-	gas	Ferrarese & Ford (1999)
NGC6300	14.2±1.4	7.14 ^{+0.20} _{-7.14}	1.94±0.02	10.98±0.11	0.74±0.09	0.05	3.9±0.3	-	gas	Beifiori et al. (2012)

Table continues on next page.

Name	Distance	M_{\bullet}	σ_e	L_k	R_e	covar.	C_{28}	AGN	method	ref.
(1)	Mpc	$\log(M_{\odot})$	$\log(\text{km s}^{-1})$	$\log(L_{\odot})$	$\log(\text{kpc})$	L_k-R_e	(8)	$\log(L_{\odot})$	(10)	(11)
NGC6323	113.4±12.3	7.00±0.05	2.20±0.07	11.25±0.09	0.91±0.05	0.05	3.3±0.2	9.45±0.14	maser	Kuo et al. (2011)
NGC6500	36.5±3.6	8.34±0.26	2.33±0.01	10.90±0.08	0.50±0.05	0.05	5.6±0.3	-	gas	Beifiori et al. (2012)
NGC6503	5.3±0.5	6.30 ^{+0.11} _{-6.30}	1.74±0.02	9.92±0.10	0.20±0.06	0.04	3.6±0.6	-	star	Kormendy et al. (2010)
NGC6814	22.3±2.2	7.02±0.17	1.98±0.01	11.04±0.10	0.68±0.06	0.05	3.7±0.4	9.54±0.02	reverb	Bentz et al. (2010)
NGC6861	27.3±4.5	9.30±0.08	2.59±0.02	11.14±0.13	0.32±0.08	0.07	5.3±0.4	-	star	Rusli et al. (2013)
NGC6951	16.0±1.6	6.93 ^{+0.19} _{-6.93}	1.98±0.04	11.01±0.14	0.85±0.13	0.05	4.7±0.8	-	gas	Beifiori et al. (2012)
NGC7052	70.4±8.4	8.60±0.23	2.42±0.02	11.68±0.09	1.00±0.05	0.05	5.7±0.3	-	gas	van der Marel & van den Bosch (1998)
NGC7331	12.2±1.2	8.02±0.18	2.06±0.02	11.14±0.10	0.57±0.08	0.05	4.6±0.4	-	gas	Beifiori et al. (2012)
NGC7332	21.7±2.2	7.08±0.18	2.10±0.02	10.81±0.08	0.40±0.07	0.04	5.9±0.3	9.11±0.14	star	Håring & Rix (2004)
NGC7418	18.4±1.8	5.18 ^{+1.78} _{-5.18}	1.67±0.06	10.60±0.11	0.75±0.10	0.05	2.5±0.4	-	star	Neumayer & Walcher (2012)
NGC7424	10.9±1.1	5.18 ^{+0.43} _{-5.18}	1.34±0.05	9.82±0.11	0.45±0.08	0.05	3.0±0.3	-	star	Neumayer & Walcher (2012)
NGC7457	12.5±1.2	6.95±0.30	1.87±0.02	10.25±0.08	0.35±0.04	0.04	3.9±0.1	-	star	Schulze & Gebhardt (2011)
NGC7582	22.3±9.8	7.74±0.20	2.19±0.05	11.21±0.32	0.89±0.19	0.16	6.6±0.4	-	gas	Wold et al. (2006)
NGC7619	51.5±7.4	9.40±0.11	2.51±0.02	11.66±0.12	0.87±0.09	0.07	5.8±0.4	-	star	Rusli et al. (2013)
NGC7626	38.1±3.8	8.58±0.33	2.37±0.02	11.44±0.09	0.87±0.08	0.05	5.4±0.3	-	gas	Beifiori et al. (2012)
NGC7682	59.3±5.9	7.56±0.33	2.05±0.06	10.96±0.10	0.80±0.10	0.06	5.1±0.4	-	gas	Beifiori et al. (2012)
NGC7768	116.0±27.5	9.13±0.18	2.42±0.02	11.91±0.19	1.15±0.12	0.10	5.7±0.4	-	star	McConnell et al. (2012)
SBS1116+583A	119.4±11.9	6.54±0.20	1.96±0.02	10.50±0.08	0.44±0.09	0.08	3.9±1.9	9.97±0.08	reverb	Bentz et al. (2010)
UGC12064	34.7±6.7	8.84±0.52	2.41±0.03	10.61±0.17	0.38±0.13	0.12	5.9±0.6	-	gas	Beifiori et al. (2012)
UGC1214	59.9±6.0	7.74 ^{+0.18} _{-7.74}	2.02±0.06	10.74±0.09	0.38±0.06	0.04	4.7±0.6	10.05±0.03	gas	Beifiori et al. (2012)
UGC1395	60.8±6.1	6.83 ^{+0.28} _{-6.83}	1.81±0.04	10.86±0.11	0.85±0.10	0.06	4.7±0.4	-	gas	Beifiori et al. (2012)
UGC1841	74.9±7.5	8.47±0.19	2.47±0.04	11.98±0.09	1.49±0.06	0.06	4.7±0.6	-	gas	Beifiori et al. (2012)
UGC3789	49.9±5.4	6.99±0.09	2.03±0.05	11.01±0.12	0.66±0.11	0.05	5.7±0.5	-	maser	Kuo et al. (2011)
UGC6093	150.0±15.0	7.41±0.02	2.19±0.05	11.40±0.08	0.97±0.05	0.05	3.8±0.3	9.26±3.14	maser	Greene et al. (2016)
UGC7115	88.2±8.8	9.00±0.45	2.25±0.08	11.24±0.09	0.54±0.07	0.06	6.1±0.9	-	gas	Beifiori et al. (2012)
UGC9799	151.1±15.1	8.89 ^{+0.80} _{-8.89}	2.37±0.02	11.99±0.09	1.37±0.06	0.05	4.5±0.3	-	gas	Dalla Bontà et al. (2009)

Objects omitted from the fits

Mrk0110	151.1±15.1	7.28±0.21	1.96±0.03	10.58±0.10	0.77±0.07	0.07	3.0±0.5	10.82±0.00	reverb	Peterson et al. (2004)
Mrk0279	130.4±13.0	7.40±0.23	2.29±0.03	11.29±0.08	0.42±0.08	0.09	5.2±0.9	11.21±0.02	reverb	Peterson et al. (2004)
NGC1068	15.9±9.4	6.92±0.25	2.18±0.02	11.32±0.40	0.32±0.20	0.20	4.6±0.4	10.62±0.02	maser	Lodato & Bertin (2003)
NGC1300	21.5±9.4	7.88±0.34	2.34±0.02	11.05±0.34	1.09±0.17	0.17	3.4±0.4	-	gas	Atkinson et al. (2005)
NGC2139	23.6±2.4	5.18 ^{+0.43} _{-5.18}	1.34±0.08	10.36±0.08	0.47±0.04	0.04	2.9±0.1	-	star	Neumayer & Walcher (2012)
NGC2911	43.5±4.3	9.09±0.29	2.32±0.03	11.28±0.10	0.88±0.12	0.08	6.3±0.3	-	gas	Beifiori et al. (2012)
NGC3516	37.9±3.8	7.37±0.16	2.26±0.01	11.11±0.11	0.40±0.13	0.10	7.1±0.8	9.98±0.11	reverb	Denney et al. (2010)
NGC4041	19.5±2.0	6.00 ^{+0.20} _{-6.00}	1.98±0.02	10.61±0.10	0.24±0.11	0.06	4.4±0.7	-	gas	Marconi et al. (2003)
NGC4636	13.7±1.4	8.58±0.22	2.26±0.02	11.25±0.09	0.96±0.08	0.06	5.5±0.4	-	gas	Beifiori et al. (2012)
NGC4699	18.9±2.1	8.25±0.05	2.26±0.01	11.38±0.11	0.49±0.12	0.08	5.6±0.6	-	stars	Saglia et al. (2016)
NGC4736	4.5±0.8	6.78±0.12	2.05±0.02	10.67±0.16	0.00±0.12	0.09	6.2±0.5	-	star	Kormendy et al. (2011)
NGC4826	5.2±1.2	6.05±0.13	1.98±0.02	10.71±0.19	0.38±0.12	0.09	4.7±0.4	-	star	Kormendy et al. (2011)
NGC5018	40.5±4.9	8.02±0.08	2.32±0.01	11.54±0.09	0.62±0.06	0.05	5.5±0.3	-	stars	Saglia et al. (2016)
NGC5194	7.9±0.8	5.96 ^{+0.36} _{-5.96}	1.84±0.06	11.04±0.10	0.73±0.08	0.05	4.9±0.6	8.36±0.23	gas	Beifiori et al. (2012)
NGC7469	47.7±8.1	6.94±0.16	2.12±0.02	11.12±0.15	-0.00±0.17	0.15	8.4±2.8	-	reverb	Peterson et al. (2014)

Table 2 Sample of the black hole mass measurements and the growth curve photometry. (1) name. (2) Distance (3) BH mass (4) stellar velocity dispersion inside the half-light radius. (5,6) total luminosity and half-light radius derived from the growth curves analysis. The photometric uncertainties include the contribution from the distance uncertainty. (7,8,9) covariance between L_k and R_e , concentration and non-stellar AGN flux from the growth curves. (10) method used for BH mass measurement. (11) Literature reference.

Name	Distance	M_{\bullet}	σ_e	L_k	R_e	covar.	C_{28}	AGN	method	ref.
(1)	Mpc	$\log(M_{\odot})$	$\log(\text{km s}^{-1})$	$\log(L_{\odot})$	$\log(\text{kpc})$	L_k-R_e	(8)	$\log(L_{\odot})$	(10)	(11)
Objects omitted due to incomplete data										
1RXSJ1858+4850	338.3	6.68±0.19	-	-	-	-	-	-	reverb	Pei et al. (2014)
H0507+164	76.57	6.69±0.36	-	-	-	-	-	-	reverb	Stalin et al. (2011)
M60UCD1	16.50	7.30±0.15	1.82±0.03	8.29	-1.62	-	-	-	star	Seth et al. (2014)
MW	0.008000	6.63±0.05	2.00±0.09	-	-	-	-	-	star	Ghez et al. (2008); Gillessen et al. (2009)
Mrk0006	80.6±8.1	8.09±0.15	-	11.11±0.09	0.66±0.08	0.06	6.0±0.6	10.99±0.01	reverb	Doroshenko et al. (2012)

Table continues on next page.

Name	Distance	M_{\bullet}	σ_e	L_k	R_e	covar.	C_{28}	AGN	method	ref.
(1)	Mpc (2)	$\log(M_{\odot})$ (3)	$\log(\text{km s}^{-1})$ (4)	$\log(L_{\odot})$ (5)	$\log(\text{kpc})$ (6)	L_k-R_e (7)	(8)	$\log(L_{\odot})$ (9)	(10)	(11)
Mrk0142	192.5	6.27±0.21	-	-	-	-	-	-	reverb	Du et al. (2014)
Mrk0290	126.7	7.26±0.17	-	-	-	-	-	-	reverb	Denney et al. (2010)
Mrk0335	110.5	7.21±0.16	-	-	-	-	-	-	reverb	Du et al. (2014)
Mrk1029	124.0	6.28±0.13	2.12±0.05	-	-	-	-	-	maser	Greene et al. (2016)
Mrk1501	382.6	8.03±0.26	-	-	-	-	-	-	reverb	Grier et al. (2012)
NGC0224	0.7740	8.15±0.16	2.20±0.02	10.69	0.22	-	-	-	star	Bender et al. (2005)
NGC0300	2.200	2.00 ^{+3.00} _{-2.00}	1.11±0.07	9.45	0.30	-	-	-	star	Neumayer & Walcher (2012)
NGC4244	4.370	0.00 ^{+3.66} _{-0.00}	1.45±0.15	9.50	0.37	-	-	-	star	De Lorenzi et al. (2013)
NGC4395	4.400	5.54±0.54	1.47±0.07	8.61	0.01	-	-	-	gas	den Brok et al. (2015)
NGC6264	147.6	7.49±0.05	2.20±0.04	11.17	0.96	-	-	-	maser	Kuo et al. (2011)
NGC7793	3.300	3.70 ^{+2.20} _{-3.70}	1.39±0.07	9.61	0.22	-	-	-	star	Neumayer & Walcher (2012)
PG0026+129	608.2	8.46±0.22	-	-	-	-	-	-	reverb	Peterson et al. (2004)
PG0052+251	661.5	8.44±0.20	-	-	-	-	-	-	reverb	Peterson et al. (2004)
PG0804+761	428.3	8.72±0.16	-	-	-	-	-	-	reverb	Peterson et al. (2004)
PG0953+414	1003.	8.31±0.21	-	-	-	-	-	-	reverb	Peterson et al. (2004)
PG1226+023	678.1	8.81±0.21	-	-	-	-	-	-	reverb	Peterson et al. (2004)
PG1229+204	269.9	7.72±0.31	2.20±0.09	-	-	-	-	-	reverb	Peterson et al. (2004)
PG1307+085	663.8	8.49±0.24	-	-	-	-	-	-	reverb	Peterson et al. (2004)
PG1411+442	383.7	8.50±0.26	2.32±0.06	-	-	-	-	-	reverb	Peterson et al. (2004)
PG1426+015	370.8	8.96±0.25	2.34±0.03	-	-	-	-	-	reverb	Peterson et al. (2004)
PG1613+658	552.5	8.27±0.33	-	-	-	-	-	-	reverb	Peterson et al. (2004)
PG1617+175	481.6	8.63±0.22	2.30±0.08	-	-	-	-	-	reverb	Peterson et al. (2004)
PG1700+518	1251.	8.76±0.21	-	-	-	-	-	-	reverb	Peterson et al. (2004)
PG2130+099	269.7	7.41±0.17	2.21±0.05	-	-	-	-	-	reverb	Grier et al. (2012)
Zw229-015	119.4	6.88±0.21	-	-	-	-	-	-	reverb	Barth et al. (2011a)

BH mass measurements omitted because of the availability of a stellar dynamical BH mass measurement.

NGC3227	23.8±2.6	6.75±0.21	1.96±0.03	11.21±0.12	1.03±0.13	0.06	4.9±0.4	9.51±0.12	reverb	Denney et al. (2010)
NGC4151	20.0±2.8	7.54±0.16	1.99±0.01	11.00±0.11	0.62±0.12	0.08	7.1±0.4	10.23±0.03	reverb	Bentz et al. (2006)
NGC4395	4.400	5.43±0.25	1.47±0.07	8.61	0.01	-	-	-	reverb	Peterson et al. (2005)

Table 3 Sample of the black hole mass measurements that have incomplete data and are hence excluded from the fits. (1) name. (2) Distance (3) BH mass (4) stellar velocity dispersion inside the half-light radius. (5,6) total luminosity and half-light radius derived from the growth curves. The photometric uncertainties include the contribution from the distance uncertainty. When no uncertainties are listed, the values comes from the LGA (Jarrett et al. 2003), XSC (Jarrett et al. 2000) or their literature source. (7,8,9) covariance between L_k and R_e , concentration and non-stellar AGN flux from the growth curves. (10) method used for BH mass measurement. (11) Literature reference.

REFERENCES

- Aller, M. C., & Richstone, D. O. 2007, *ApJ*, 665, 120
- Anglés-Alcázar, D., Özel, F., & Davé, R. 2013, *ApJ*, 770, 5
- Atkinson, J. W., Collett, J. L., Marconi, A., et al. 2005, *MNRAS*, 359, 504
- Auger, M. W., Treu, T., Bolton, A. S., et al. 2010, *ApJ*, 724, 511
- Baldassare, V. F., Reines, A. E., Gallo, E., & Greene, J. E. 2015, *ApJL*, 809, L14
- Barth, A. J., Boizelle, B. D., Darling, J., et al. 2016, *ApJL*, 822, L28
- Barth, A. J., Ho, L. C., Filippenko, A. V., Rix, H.-W., & Sargent, W. L. W. 2001, *ApJ*, 546, 205
- Barth, A. J., Strigari, L. E., Bentz, M. C., Greene, J. E., & Ho, L. C. 2009, *ApJ*, 690, 1031
- Barth, A. J., Nguyen, M. L., Malkan, M. A., et al. 2011a, *ApJ*, 732, 121
- Barth, A. J., Pancoast, A., Thorman, S. J., et al. 2011b, *ApJL*, 743, L4
- Barth, A. J., Pancoast, A., Bennert, V. N., et al. 2013, *ApJ*, 769, 128
- Barway, S., & Kembhavi, A. 2007, *ApJL*, 662, L67
- Batcheldor, D. 2010, *ApJL*, 711, L108
- Beifiori, A., Courteau, S., Corsini, E. M., & Zhu, Y. 2012, *MNRAS*, 419, 2497
- Beifiori, A., Sarzi, M., Corsini, E. M., et al. 2009, *ApJ*, 692, 856
- Bell, E. F., & de Jong, R. S. 2001, *ApJ*, 550, 212
- Bellovary, J. M., Holley-Bockelmann, K., Gültekin, K., et al. 2014, *MNRAS*, 445, 2667
- Bender, R., Kormendy, J., Bower, G., et al. 2005, *ApJ*, 631, 280
- Bennert, V. N., Auger, M. W., Treu, T., Woo, J.-H., & Malkan, M. A. 2011, *ApJ*, 726, 59
- Bentz, M. C., & Katz, S. 2015, *PASP*, 127, 67
- Bentz, M. C., Denney, K. D., Cackett, E. M., et al. 2006, *ApJ*, 651, 775
- Bentz, M. C., Walsh, J. L., Barth, A. J., et al. 2010, *ApJ*, 716, 993
- Bentz, M. C., Horenstein, D., Bazhaw, C., et al. 2014, *ApJ*, 796, 8
- Berrier, J. C., Davis, B. L., Kennefick, D., et al. 2013, *ApJ*, 769, 132
- Bershady, M. A., Martinsson, T. P. K., Verheijen, M. A. W., et al. 2011, *ApJL*, 739, L47
- Bertin, E. 2011, in *Astronomical Society of the Pacific Conference Series, Vol. 442, Astronomical Data Analysis Software and Systems XX*, ed. I. N. Evans, A. Accomazzi, D. J. Mink, & A. H. Rots, 435
- Bertin, E., & Arnouts, S. 1996, *A&AS*, 117, 393
- Bezanson, R., Franx, M., & van Dokkum, P. G. 2015, *ApJ*, 799, 148
- Bezanson, R., van Dokkum, P., & Franx, M. 2012, *ApJ*, 760, 62
- Bianchini, P., Norris, M. A., van de Ven, G., & Schinnerer, E. 2015, *MNRAS*, 453, 365
- Blais-Ouellette, S., Amram, P., Carignan, C., & Swaters, R. 2004, *A&A*, 420, L147
- Bolton, A. S., Treu, T., Koopmans, L. V. E., et al. 2008, *ApJ*, 684, 248
- Bower, G. A., Green, R. F., Bender, R., et al. 2001, *ApJ*, 550, 75
- Braatz, J., Greenhill, L., Moran, J., Wilson, A., & Herrnstein, J. 1997, in *Bulletin of the American Astronomical Society, Vol. 29, American Astronomical Society Meeting Abstracts*, 1374
- Capetti, A., Marconi, A., Macchetto, D., & Axon, D. 2005, *A&A*, 431, 465
- Cappellari, M. 2016, *ArXiv e-prints*, arXiv:1602.04267
- Cappellari, M., Verolme, E. K., van der Marel, R. P., et al. 2002, *ApJ*, 578, 787
- Cappellari, M., Bacon, R., Bureau, M., et al. 2006, *MNRAS*, 366, 1126
- Cappellari, M., Bacon, R., Davies, R. L., et al. 2008, in *IAU Symposium, Vol. 245, Formation and Evolution of Galaxy Bulges*, ed. M. Bureau, E. Athanassoula, & B. Barbuy, 215
- Cappellari, M., di Serego Alighieri, S., Cimatti, A., et al. 2009, *ApJL*, 704, L34
- Cappellari, M., Emsellem, E., Krajnović, D., et al. 2011, *MNRAS*, 413, 813
- Cappellari, M., Scott, N., Alatalo, K., et al. 2013a, *MNRAS*, 432, 1709
- Cappellari, M., McDermid, R. M., Alatalo, K., et al. 2013b, *MNRAS*, 432, 1862
- Chen, C.-W., Côté, P., West, A. A., Peng, E. W., & Ferrarese, L. 2010, *ApJL*, 719, L1
- Coccatto, L., Sarzi, M., Pizzella, A., et al. 2006, *MNRAS*, 366, 1050
- Courteau, S., & Dutton, A. A. 2015, *ApJL*, 801, L20
- Courteau, S., Dutton, A. A., van den Bosch, F. C., et al. 2007a, *ApJ*, 671, 203

- Courteau, S., McDonald, M., Widrow, L. M., & Holtzman, J. 2007b, *ApJL*, 655, L21
- Courteau, S., Cappellari, M., de Jong, R. S., et al. 2014, *Reviews of Modern Physics*, 86, 47
- Cretton, N., & van den Bosch, F. C. 1999, *ApJ*, 514, 704
- Dalla Bontà, E., Ferrarese, L., Corsini, E. M., et al. 2009, *ApJ*, 690, 537
- Davies, R. I., Thomas, J., Genzel, R., et al. 2006, *ApJ*, 646, 754
- Davis, T. A. 2014, *MNRAS*, 443, 911
- Davis, T. A., Bureau, M., Cappellari, M., Sarzi, M., & Blitz, L. 2013, *Nature*, 494, 328
- de Francesco, G., Capetti, A., & Marconi, A. 2008, *A&A*, 479, 355
- De Lorenzi, F., Hartmann, M., Debattista, V. P., Seth, A. C., & Gerhard, O. 2013, *MNRAS*, 429, 2974
- den Brok, M., van de Ven, G., van den Bosch, R., & Watkins, L. 2014, *MNRAS*, 438, 487
- den Brok, M., Seth, A. C., Barth, A. J., et al. 2015, *ApJ*, 809, 101
- Denney, K. D., Watson, L. C., Peterson, B. M., et al. 2009, *ApJ*, 702, 1353
- Denney, K. D., Peterson, B. M., Pogge, R. W., et al. 2010, *ApJ*, 721, 715
- Devereux, N., Ford, H., Tsvetanov, Z., & Jacoby, G. 2003, *AJ*, 125, 1226
- Dietrich, M., Peterson, B. M., Grier, C. J., et al. 2012, *ApJ*, 757, 53
- Djorgovski, S., & Davis, M. 1987, *ApJ*, 313, 59
- Do, T., Wright, S. A., Barth, A. J., et al. 2014, *AJ*, 147, 93
- Doroshenko, V. T., Sergeev, S. G., Klimanov, S. A., Pronik, V. I., & Efimov, Y. S. 2012, *MNRAS*, 426, 416
- Doroshenko, V. T., Sergeev, S. G., & Pronik, V. I. 2008, *Astronomy Reports*, 52, 442
- Dressler, A., Lynden-Bell, D., Burstein, D., et al. 1987, *ApJ*, 313, 42
- Du, P., Hu, C., Lu, K.-X., et al. 2014, *ApJ*, 782, 45
- Emsellem, E., Dejonghe, H., & Bacon, R. 1999, *MNRAS*, 303, 495
- Emsellem, E., Cappellari, M., Peletier, R. F., et al. 2004, *MNRAS*, 352, 721
- Faber, S. M., & Jackson, R. E. 1976, *ApJ*, 204, 668
- Fabian, A. C. 1999, *MNRAS*, 308, L39
- Falcón-Barroso, J., Lyubenova, M., Van de Ven, G., & the CALIFA team. 2016, *A&A*, submitted
- Falcón-Barroso, J., van de Ven, G., Peletier, R. F., et al. 2011, *MNRAS*, 417, 1787
- Feoli, A., & Mancini, L. 2009, *ApJ*, 703, 1502
- Feoli, A., Mancini, L., Marulli, F., & van den Bergh, S. 2011, *General Relativity and Gravitation*, 43, 1007
- Ferrarese, L., & Ford, H. 2005, *Space Sci. Rev.*, 116, 523
- Ferrarese, L., & Ford, H. C. 1999, *ApJ*, 515, 583
- Ferrarese, L., Ford, H. C., & Jaffe, W. 1996, *ApJ*, 470, 444
- Ferrarese, L., Côté, P., Dalla Bontà, E., et al. 2006, *ApJL*, 644, L21
- Ferré-Mateu, A., Mezcuca, M., Trujillo, I., Balcells, M., & van den Bosch, R. C. E. 2015, *ApJ*, 808, 79
- Frank, M. J., Hilker, M., Mieske, S., et al. 2011, *MNRAS*, 414, L70
- Gao, F., Braatz, J. A., Reid, M. J., et al. 2016, *ApJ*, 817, 128
- Gebhardt, K., Rich, R. M., & Ho, L. C. 2005, *ApJ*, 634, 1093
- Gebhardt, K., Lauer, T. R., Kormendy, J., et al. 2001, *AJ*, 122, 2469
- Gebhardt, K., Richstone, D., Tremaine, S., et al. 2003, *ApJ*, 583, 92
- Gebhardt, K., Lauer, T. R., Pinkney, J., et al. 2007, *ApJ*, 671, 1321
- Ghez, A. M., Salim, S., Weinberg, N. N., et al. 2008, *ApJ*, 689, 1044
- Gillessen, S., Eisenhauer, F., Trippe, S., et al. 2009, *ApJ*, 692, 1075
- Graham, A. W. 2008, *ApJ*, 680, 143
- . 2016, *Galactic Bulges*, 418, 263
- Graham, A. W., & Scott, N. 2013, *ApJ*, 764, 151
- Graves, G. J., & Faber, S. M. 2010, *ApJ*, 717, 803
- Greene, J. E., & Ho, L. C. 2007, *ApJ*, 670, 92
- Greene, J. E., Peng, C. Y., Kim, M., et al. 2010, *ApJ*, 721, 26
- Greene, J. E., Seth, A. C., Kim, M., et al. 2016, *ArXiv e-prints*, arXiv:1606.00018
- Greenhill, L. J., Moran, J. M., & Herrnstein, J. R. 1997, *ApJL*, 481, L23
- Greenhill, L. J., Booth, R. S., Ellingsen, S. P., et al. 2003, *ApJ*, 590, 162
- Grier, C. J., Peterson, B. M., Pogge, R. W., et al. 2012, *ApJ*, 755, 60
- Grier, C. J., Martini, P., Watson, L. C., et al. 2013, *ApJ*, 773, 90
- Gültekin, K., Gebhardt, K., Kormendy, J., et al. 2014, *ApJ*, 781, 112
- Gültekin, K., Tremaine, S., Loeb, A., & Richstone, D. O. 2011, *ApJ*, 738, 17
- Gültekin, K., Richstone, D. O., Gebhardt, K., et al. 2009a, *ApJ*, 695, 1577
- . 2009b, *ApJ*, 698, 198
- Haggard, D., Cool, A. M., Heinke, C. O., et al. 2013, *ApJL*, 773, L31
- Häring, N., & Rix, H.-W. 2004, *ApJL*, 604, L89
- Harris, G. L. H., & Harris, W. E. 2011, *MNRAS*, 410, 2347
- Herrnstein, J. R., Moran, J. M., Greenhill, L. J., & Trotter, A. S. 2005, *ApJ*, 629, 719
- Ho, L. C. 2007, *ApJ*, 668, 94
- Hopkins, P. F., Bundy, K., Hernquist, L., & Ellis, R. S. 2007a, *ApJ*, 659, 976
- Hopkins, P. F., Hernquist, L., Cox, T. J., Robertson, B., & Krause, E. 2007b, *ApJ*, 669, 67
- Hopkins, P. F., Lidz, A., Hernquist, L., et al. 2007c, *ApJ*, 662, 110
- Houghton, R. C. W., Magorrian, J., Sarzi, M., et al. 2006, *MNRAS*, 367, 2
- Hu, J. 2009, *ArXiv e-prints*, arXiv:0908.2028 [astro-ph.GA]
- Huang, S., Ho, L. C., Peng, C. Y., Li, Z.-Y., & Barth, A. J. 2013, *ApJ*, 766, 47
- Huré, J.-M., Hersant, F., Surville, C., Nakai, N., & Jacq, T. 2011, *A&A*, 530, A145
- Jahnke, K., & Macciò, A. V. 2011, *ApJ*, 734, 92
- Janz, J., Norris, M. A., Forbes, D. A., et al. 2016, *MNRAS*, 456, 617
- Jardel, J. R., Gebhardt, K., Shen, J., et al. 2011, *ApJ*, 739, 21
- Jarrett, T. H., Chester, T., Cutri, R., et al. 2000, *AJ*, 119, 2498
- Jarrett, T. H., Chester, T., Cutri, R., Schneider, S. E., & Huchra, J. P. 2003, *AJ*, 125, 525
- Jiang, Y.-F., Greene, J. E., & Ho, L. C. 2011, *ApJL*, 737, L45
- Kamann, S., Wisotzki, L., Roth, M. M., et al. 2014, *A&A*, 566, A58
- Kamann, S., Husser, T.-O., Brinchmann, J., et al. 2016, *A&A*, 588, A149
- Kelly, B. C. 2007, *ApJ*, 665, 1489
- Kelly, B. C., & Merloni, A. 2012, *Advances in Astronomy*, 2012, 7
- King, A. 2003, *ApJL*, 596, L27
- Kollatschny, W., Ulbrich, K., Zetzl, M., Kaspi, S., & Haas, M. 2014, *A&A*, 566, A106
- Kondratko, P. T., Greenhill, L. J., & Moran, J. M. 2005, *ApJ*, 618, 618
- . 2008, *ApJ*, 678, 87
- Kormendy, J. 1977, *ApJ*, 218, 333
- Kormendy, J., & Bender, R. 2009, *ApJL*, 691, L142
- . 2011, *Nature*, 469, 377
- Kormendy, J., Bender, R., & Cornell, M. E. 2011, *Nature*, 469, 374
- Kormendy, J., Drory, N., Bender, R., & Cornell, M. E. 2010, *ApJ*, 723, 54
- Kormendy, J., Fisher, D. B., Cornell, M. E., & Bender, R. 2009, *ApJS*, 182, 216
- Kormendy, J., & Ho, L. C. 2013, *ARA&A*, 51, 511
- Kormendy, J., & Kennicutt, Jr., R. C. 2004, *ARA&A*, 42, 603
- Kovačević, A., Popović, L. Č., Shapovalova, A. I., et al. 2014, *Advances in Space Research*, 54, 1414
- Krajinović, D., McDermid, R. M., Cappellari, M., & Davies, R. L. 2009, *MNRAS*, 399, 1839
- Kuo, C. Y., Braatz, J. A., Condon, J. J., et al. 2011, *ApJ*, 727, 20
- Lanzoni, B., Mucciarelli, A., Origlia, L., et al. 2013, *ApJ*, 769, 107
- Läsker, R., Ferrarese, L., & van de Ven, G. 2014a, *ApJ*, 780, 69
- Läsker, R., Ferrarese, L., van de Ven, G., & Shankar, F. 2014b, *ApJ*, 780, 70
- Läsker, R., Greene, J. E., Seth, A., et al. 2016, *ArXiv e-prints*, arXiv:1602.06960
- Läsker, R., van den Bosch, R. C. E., van de Ven, G., et al. 2013, *MNRAS*, 434, L31
- Lauer, T. R., Tremaine, S., Richstone, D., & Faber, S. M. 2007a, *ApJ*, 670, 249
- Lauer, T. R., Faber, S. M., Richstone, D., et al. 2007b, *ApJ*, 662, 808
- Lodato, G., & Bertin, G. 2003, *A&A*, 398, 517
- Lützgendorf, N., Gebhardt, K., Baumgardt, H., et al. 2015, *A&A*, 581, A1
- Lützgendorf, N., Kissler-Patig, M., Noyola, E., et al. 2011, *A&A*, 533, A36
- Lützgendorf, N., Kissler-Patig, M., Gebhardt, K., et al. 2013, *A&A*, 552, A49
- Lyubenova, M., van den Bosch, R. C. E., Côté, P., et al. 2013, *MNRAS*, 431, 3364
- Marconi, A., & Hunt, L. K. 2003, *ApJL*, 589, L21
- Marconi, A., Axon, D. J., Capetti, A., et al. 2003, *ApJ*, 586, 868
- McConnell, N. J., & Ma, C.-P. 2013, *ApJ*, 764, 184
- McConnell, N. J., Ma, C.-P., Gebhardt, K., et al. 2011a, *Nature*, 480, 215
- McConnell, N. J., Ma, C.-P., Graham, J. R., et al. 2011b, *ApJ*, 728, 100
- McConnell, N. J., Ma, C.-P., Murphy, J. D., et al. 2012, *ApJ*, 756, 179
- McLaughlin, D. E., Anderson, J., Meylan, G., et al. 2006, *ApJS*, 166, 249
- McNamara, B. R., & Nulsen, P. E. J. 2012, *New Journal of Physics*, 14, 055023
- Medling, A. M., Ammons, S. M., Max, C. E., et al. 2011, *ApJ*, 743, 32
- Meidt, S. E., Schinnerer, E., van de Ven, G., et al. 2014, *ApJ*, 788, 144
- Merritt, D., Ferrarese, L., & Joseph, C. L. 2001, *Science*, 293, 1116
- Mieske, S., Frank, M. J., Baumgardt, H., et al. 2013, *A&A*, 558, A14
- Miller-Jones, J. C. A., Wrobel, J. M., Sivakoff, G. R., et al. 2012, *ApJL*, 755, L1
- Misgeld, I., Mieske, S., Hilker, M., et al. 2011, *A&A*, 531, A4
- Neumayer, N., & Walcher, C. J. 2012, *Advances in Astronomy*, 2012, 15
- Nguyen, D. D., Seth, A. C., Reines, A. E., et al. 2014, *ApJ*, 794, 34
- Norris, M. A., Escudero, C. G., Faifer, F. R., et al. 2015, *MNRAS*, 451, 3615
- Norris, M. A., Meidt, S., van de Ven, G., et al. 2014a, *ApJ*, 797, 55
- Norris, M. A., Kannappan, S. J., Forbes, D. A., et al. 2014b, *MNRAS*, 443, 1151
- Nowak, N., Saglia, R. P., Thomas, J., et al. 2008, *MNRAS*, 391, 1629
- . 2007, *MNRAS*, 379, 909
- Nowak, N., Thomas, J., Erwin, P., et al. 2010, *MNRAS*, 403, 646
- Noyola, E., Gebhardt, K., Kissler-Patig, M., et al. 2010, *ApJL*, 719, L60
- Onishi, K., Iguchi, S., Davis, T. A., et al. 2016, *MNRAS*, submitted
- Onishi, K., Iguchi, S., Sheth, K., & Kohno, K. 2015, *ApJ*, 806, 39
- Onken, C. A., & Peterson, B. M. 2002, *ApJ*, 572, 746
- Onken, C. A., Valluri, M., Brown, J. S., et al. 2014, *ApJ*, 791, 37
- Park, D., Kelly, B. C., Woo, J.-H., & Treu, T. 2012, *ApJS*, 203, 6
- Pastorini, G., Marconi, A., Capetti, A., et al. 2007, *A&A*, 469, 405
- Paturel, G., Andermach, H., Bottinelli, L., et al. 1997, *A&AS*, 124, 109
- Pei, L., Barth, A. J., Aldering, G. S., et al. 2014, *ApJ*, 795, 38
- Peng, C. Y. 2007, *ApJ*, 671, 1098
- Peng, C. Y., Ho, L. C., Impey, C. D., & Rix, H.-W. 2002, *AJ*, 124, 266
- Peterson, B. M. 2014, *Space Sci. Rev.*, 183, 253
- Peterson, B. M., Ferrarese, L., Gilbert, K. M., et al. 2004, *ApJ*, 613, 682
- Peterson, B. M., Bentz, M. C., Desroches, L.-B., et al. 2005, *ApJ*, 632, 799
- Peterson, B. M., Grier, C. J., Horne, K., et al. 2014, *ApJ*, 795, 149
- Pignatelli, E., Salucci, P., & Danese, L. 2001, *MNRAS*, 320, 124
- Reines, A. E., Greene, J. E., & Geha, M. 2013, *ApJ*, 775, 116
- Reines, A. E., Sivakoff, G. R., Johnson, K. E., & Brogan, C. L. 2011, *Nature*, 470, 66

- Reines, A. E., & Volonteri, M. 2015, *ApJ*, 813, 82
- Rusli, S. P., Thomas, J., Saglia, R. P., et al. 2013, *AJ*, 146, 45
- Saglia, R. P., Opitsch, M., Erwin, P., et al. 2016, *ApJ*, 818, 47
- Sani, E., Marconi, A., Hunt, L. K., & Risaliti, G. 2011, *MNRAS*, 413, 1479
- Sartori, L. F., Schawinski, K., Treister, E., et al. 2015, *MNRAS*, 454, 3722
- Sarzi, M., Rix, H.-W., Shields, J. C., et al. 2001, *ApJ*, 550, 65
- Savorgnan, G., Graham, A. W., Marconi, A., et al. 2013, *MNRAS*, 434, 387
- Savorgnan, G. A. D., & Graham, A. W. 2016, *ApJS*, 222, 10
- Savorgnan, G. A. D., Graham, A. W., Marconi, A., & Sani, E. 2016, *ApJ*, 817, 21
- Scharwächter, J., McGregor, P. J., Dopita, M. A., & Beck, T. L. 2013, *MNRAS*, 429, 2315
- Schaye, J., Crain, R. A., Bower, R. G., et al. 2015, *MNRAS*, 446, 521
- Schlegel, D. J., Finkbeiner, D. P., & Davis, M. 1998, *ApJ*, 500, 525
- Schulze, A., & Gebhardt, K. 2011, *ApJ*, 729, 21
- Seth, A. C., Cappellari, M., Neumayer, N., et al. 2010, *ApJ*, 714, 713
- Seth, A. C., van den Bosch, R., Mieske, S., et al. 2014, *Nature*, 513, 398
- Shankar, F., Weinberg, D. H., & Miralda-Escudé, J. 2009, *ApJ*, 690, 20
- Shankar, F., Bernardi, M., Sheth, R. K., et al. 2016, *MNRAS*, arXiv:1603.01276
- Shen, J., & Gebhardt, K. 2010, *ApJ*, 711, 484
- Sheth, R. K., Bernardi, M., Schechter, P. L., et al. 2003, *ApJ*, 594, 225
- Silk, J., & Rees, M. J. 1998, *A&A*, 331, L1
- Skrutskie, M. F., Cutri, R. M., Stiening, R., et al. 2006, *AJ*, 131, 1163
- Smith, R. J. 2014, *MNRAS*, 443, L69
- Stalin, C. S., Jeyakumar, S., Coziol, R., Pawase, R. S., & Thakur, S. S. 2011, *MNRAS*, 416, 225
- Steinborn, L. K., Dolag, K., Hirschmann, M., Prieto, M. A., & Remus, R.-S. 2015, *MNRAS*, 448, 1504
- Strader, J., Chomiuk, L., Maccarone, T. J., et al. 2012, *ApJL*, 750, L27
- Sun, A.-L., Greene, J. E., Impellizzeri, C. M. V., et al. 2013, *ApJ*, 778, 47
- Tadhunter, C., Marconi, A., Axon, D., et al. 2003, *MNRAS*, 342, 861
- Taylor, E. N., Franx, M., Brinchmann, J., van der Wel, A., & van Dokkum, P. G. 2010, *ApJ*, 722, 1
- Thomas, J., Ma, C.-P., McConnell, N. J., et al. 2016, *Nature*, 532, 340
- Tremaine, S., Gebhardt, K., Bender, R., et al. 2002, *ApJ*, 574, 740
- Trotter, A. S., Greenhill, L. J., Moran, J. M., et al. 1998, *ApJ*, 495, 740
- Tully, R. B., & Fisher, J. R. 1977, *A&A*, 54, 661
- Valluri, M., Ferrarese, L., Merritt, D., & Joseph, C. L. 2005, *ApJ*, 628, 137
- van de Ven, G., van den Bosch, R. C. E., Verolme, E. K., & de Zeeuw, P. T. 2006, *A&A*, 445, 513
- van den Bosch, R., de Zeeuw, T., Gebhardt, K., Noyola, E., & van de Ven, G. 2006, *ApJ*, 641, 852
- van den Bosch, R. C. E., & de Zeeuw, P. T. 2010, *MNRAS*, 401, 1770
- van den Bosch, R. C. E., Gebhardt, K., Gültekin, K., Yıldırım, A., & Walsh, J. L. 2015, *ApJS*, 218, 10
- van den Bosch, R. C. E., Greene, J. E., Braatz, J. A., Constantin, A., & Kuo, C.-Y. 2016, *ApJ*, 819, 11
- van der Marel, R. P., & Anderson, J. 2010, *ApJ*, 710, 1063
- van der Marel, R. P., & van den Bosch, F. C. 1998, *AJ*, 116, 2220
- van der Wel, A., Franx, M., van Dokkum, P. G., et al. 2014, *ApJ*, 788, 28
- Vika, M., Driver, S. P., Cameron, E., Kelvin, L., & Robotham, A. 2012, *MNRAS*, 419, 2264
- Volonteri, M., Dubois, Y., Pichon, C., & Devriendt, J. 2016, *ArXiv e-prints*, arXiv:1602.01941
- Walsh, J. L., Barth, A. J., Ho, L. C., & Sarzi, M. 2013, *ApJ*, 770, 86
- Walsh, J. L., Barth, A. J., & Sarzi, M. 2010, *ApJ*, 721, 762
- Walsh, J. L., van den Bosch, R. C. E., Barth, A. J., & Sarzi, M. 2012, *ApJ*, 753, 79
- Walsh, J. L., van den Bosch, R. C. E., Gebhardt, K., et al. 2015, *ApJ*, 808, 183
- , 2016, *ApJ*, 817, 2
- Watkins, L. L., van de Ven, G., den Brok, M., & van den Bosch, R. C. E. 2013, *MNRAS*, 436, 2598
- Wilson, A. S., Baldwin, J. A., Sun, S.-D., & Wright, A. E. 1986, *ApJ*, 310, 121
- Wold, M., Lacy, M., Käuff, H. U., & Siebenmorgen, R. 2006, *A&A*, 460, 449
- Woo, J.-H., Schulze, A., Park, D., et al. 2013, *ApJ*, 772, 49
- Yamauchi, A., Nakai, N., Sato, N., & Diamond, P. 2004, *PASJ*, 56, 605
- Yıldırım, A., van den Bosch, R. C. E., van de Ven, G., et al. 2015, *MNRAS*, 452, 1792
- Yoshii, Y., Kobayashi, Y., Minezaki, T., Koshida, S., & Peterson, B. A. 2014, *ApJL*, 784, L11
- Yu, Q., & Tremaine, S. 2002, *MNRAS*, 335, 965
- Zaritsky, D., Gonzalez, A. H., & Zabludoff, A. I. 2006, *ApJ*, 638, 725
- Zaritsky, D., Zabludoff, A. I., & Gonzalez, A. H. 2008, *ApJ*, 682, 68
- Zocchi, A., Gieles, M., & Hénault-Brunet, V. 2016, in *IAU Symposium*, Vol. 312, IAU Symposium, ed. Y. Meiron, S. Li, F.-K. Liu, & R. Spurzem, 197

APPENDIX

A. BLACK HOLE MEASUREMENTS IN GLOBULAR CLUSTERS

This appendix contains table A1 that lists a compilation of BH mass measurements in globular clusters.

Name	Distance Mpc	M_{\bullet} log(M_{\odot})	σ_e log(km s $^{-1}$)	L_k log(L_{\odot})	R_e log(kpc)	covar. L_k-R_e	C_{28}	AGN log(L_{\odot})	method	ref.
G1	0.7300	5.24±0.12	1.39±0.09	-	-	-	-	-	GC	Gebhardt et al. (2005)
NGC0104	0.004000	3.00 $^{+0.18}_{-3.00}$	1.06±0.03	5.80±0.19	-2.57±0.26	0.10	4.4±0.8	-	GC	McLaughlin et al. (2006)
NGC1851	0.01210	0.00 $^{+3.30}_{-0.00}$	0.97±0.02	5.49±0.08	-2.77±0.06	0.05	4.5±0.3	-	GC	Lützgendorf et al. (2013)
NGC1904	0.01290	3.48 $^{+0.12}_{-3.48}$	0.90±0.03	5.25±0.10	-2.42±0.10	0.05	4.8±0.6	-	GC	Lützgendorf et al. (2013)
NGC5139	0.004000	3.94 $^{+0.14}_{-3.94}$	1.28±0.03	5.70±0.13	-2.46±0.08	0.13	3.4±0.7	-	GC	van der Marel & Anderson (2010)
NGC5272	0.01020	0.00 $^{+3.72}_{-0.00}$	0.73±0.08	5.58	-2.57	-	-	-	GC	Kamann et al. (2014)
NGC5694	0.03470	0.00 $^{+3.90}_{-0.00}$	0.94±0.03	5.28±0.09	-2.42±0.08	0.05	4.8±0.6	-	GC	Lützgendorf et al. (2013)
NGC5824	0.03200	0.00 $^{+3.78}_{-0.00}$	1.05±0.02	5.70±0.09	-2.57±0.07	0.05	5.2±0.4	-	GC	Lützgendorf et al. (2013)
NGC6093	0.01000	0.00 $^{+3.00}_{-0.00}$	0.97±0.01	5.36±0.08	-2.77±0.05	0.04	4.2±0.2	-	GC	Lützgendorf et al. (2013)
NGC6205	0.007100	0.00 $^{+3.93}_{-0.00}$	0.85±0.06	5.44±0.11	-2.43±0.09	0.04	3.9±0.9	-	GC	Kamann et al. (2014)
NGC6266	0.006900	3.30 $^{+0.18}_{-3.30}$	1.19±0.01	5.77±0.09	-2.61±0.06	0.05	4.6±0.4	-	GC	Lützgendorf et al. (2013); McNamara & Nulsen (2012)
NGC6341	0.008300	0.00 $^{+2.99}_{-0.00}$	0.77±0.07	5.20±0.07	-2.71±0.05	0.04	4.0±0.3	-	GC	Kamann et al. (2014)
NGC6388	0.01160	4.23 $^{+0.18}_{-4.23}$	1.28±0.01	6.13±0.09	-2.66±0.05	0.05	5.0±0.3	-	GC	Lützgendorf et al. (2011)
NGC6397	0.002500	2.78 $^{+0.12}_{-2.78}$	0.69±0.09	4.71±0.12	-2.24±0.10	0.12	4.1±0.3	-	GC	Kamann et al. (2016)
NGC7078	0.01080	2.70 $^{+0.78}_{-2.70}$	1.10±0.20	5.59±0.08	-2.60±0.05	0.04	4.2±0.2	-	GC	van den Bosch et al. (2006); den Brok et al. (2014)

Table A1

BH mass measurements in Globular Clusters. The columns are the same as table 2. Photometry for NGC 5272 is from 2MASS LGA (Jarrett et al. 2003), the remainder is derived using the growth-curves.